https://doi.org/10.1016/j.engstruct.2021.112192

Web crippling design of lean duplex stainless steel tubular members under interior loading conditions

Yancheng Cai [*], Ben Young

[a] *Department of Civil and Environmental Engineering, The Hong Kong Polytechnic University, Hong Kong*

Abstract

Numerical analysis and design of cold-formed lean duplex stainless steel (CFLDSS) tubular members undergoing web crippling are presented in this paper. The tubular members were subjected to the loading conditions of Interior-One-Flange (IOF), Interior-Two-Flange (ITF) and Interior Loading (IL). Finite element (FE) models were developed to simulate the members under these three interior loading conditions. The results obtained from the FE analysis were used to compare with test results in terms of failure modes, strengths and load-deformation curves. After successful verification, the FE models were employed for an extensive parametric study. The key parameters in the parametric study included the ratios of flat web height to thickness, load bearing length to web thickness, load bearing length to flat web height and section inner radius. The parametric study results together with the test results were used to compare with the nominal strengths predicted by using the current specifications (ASCE, AS/NZS, NAS and EC3), and the design equations in the literature. New sets of coefficients are proposed for the unified design equation in NAS and the direct strength method (DSM) for the web crippling design of CFLDSS tubular members. Overall, the modified design rules were able to provide more accurate predictions compared with the design rules in current specifications and literature. The results showed that the proposed design methods are suitable for the design of web crippling of CFLDSS tubular members under the IOF, ITF and IL conditions.

Keywords: Direct strength method, finite element analysis, lean duplex, interior loading conditions, web crippling, tubular members.

[*] Corresponding author. Tel.: +852-3800-8475.
E-mail address: yancheng.cai@polyu.edu.hk (Y. Cai).

1. Introduction

Cold-formed steel tubular members with slender webs may buckle under high concentrated bearing loads [1]. Unlike open sections, such as channel sections, the webs of tubular members are not easy to be stiffened. Hence, their strengths against web crippling failure need be checked carefully under concentrated bearing loads. It is quite complex in the strength calculation of web crippling by means of theoretical analysis [2]. The web crippling design rules for steel tubular members are empirical in nature in most of the current design specifications.

The material cost of stainless steel is higher than that of carbon steel. The relatively new stainless steel material, lean duplex stainless steel, offers comparable high strength but lower cost than the counterpart of duplex stainless steel. It still has attractive characteristics in appearance, corrosion resistance as well as low life cycle costs [3]. The lean duplex stainless steel has gained significant attention by researchers as reflected in the wide investigations of its structural behaviour, including material properties [4-6], beams [7-9], columns [10-12], plate girders [13-14], single shear bolted connections [15-17] and double shear bolted connections [15,18]. These research achievements have led to the significant development in unlocking its design and application in construction industry. However, the lean duplex stainless steel is not covered in the current design specifications, such as American Society of Civil Engineers Specification (ASCE) [19] and the Australian/ New Zealand Standard (AS/NZS) [20] specifications, while it was introduced in the recent European Code (EC3-1.4) [21].

The cold-formed lean duplex stainless steel (CFLDSS) tubular members undergoing web crippling were experimentally investigated by Cai and Young [22,23]. Over 100 tests under different loading cases were conducted [22,23]. It is shown that the strengths predicted by using the design rules in stainless steel specifications [19-21] and carbon steel specification [24], and those in the literature [25] generally underestimated the web crippling strengths of CFLDSS tubular members, including those subjected to the concentrated bearing loadings of Interior-One-Flange (IOF), Interior-Two-Flange (ITF) and Interior Loading (IL) [23]. It should be noted that, up-to-date, limited research have been conducted on the web crippling behaviour of CFLDSS tubular members subjected to IOF, ITF and IL conditions.

Web crippling behaviour of other stainless steel grades have been investigated, including austenitic stainless steel [26-29], ferritic stainless steel [30-32] and duplex stainless steel [1,33]. In these investigations, the stainless steel tubular members were subjected to different loading conditions, including the loading conditions of End-One-Flange (EOF) [29,30,32,33], End-Two-Flange (ETF) [27,32,33] and End Loading (EL) [1,31], as well as IOF [26,28,30,32,33], ITF [27,28,32,33] and IL [1,31]. Efforts have been made to develop the design rules for web crippling of stainless steel tubular members, for examples, web crippling of ferritic stainless steel [31,32], austenitic and duplex stainless steel [25]. However, the codified web crippling design rules (ASCE [19], AS/NZS [20], EC3-1.4 [21]) for stainless steel members are mainly based on those for carbon steel members. This paper aims to develop the web crippling design of CFLDSS tubular members. The CFLDSS tubular members were subjected to IOF, ITF and IL concentrated bearing loads.

Numerical analysis and design rules for CFLDSS tubular members undergoing web crippling are presented herein. Firstly, finite element models (FEMs) were developed, and their accuracy were verified in terms of web crippling strengths, failure modes and load-deformation curves. The experimental results reported by Cai and Young [23] were used to verify the FEMs. Secondly, an extensive parametric study on 144 CFLDSS specimens was performed by using the verified FEMs. In the parametric study, the critical parameters such as the ratios of flat web height to thickness, load bearing length to web thickness, load bearing length to flat web height and sectional corner radius were considered. Thirdly, the current web crippling design rules (ASCE [19], AS/NZS [20], EC-1.4 [21] and NAS [24]), as well as the design rules in the literature [25,31,32] were assessed. Lastly, new sets of coefficients are proposed for the modification of the unified design equation specified in the NAS [24] and the direct strength method (DSM) in the literature [31,32]. The modified unified design equation and the DSM are suitable for the web crippling design of CFLDSS tubular members under the concentrated ITF, IOF and IL bearing loads. The current and modified design rules were also examined by reliability analysis.

2. Summary of experimental program

The experimental program carried out by Cai and Young [23] provided the web crippling strengths, failure modes and load-deformation curves of the CFLDSS tubular members. The CFLDSS tubular members were tested under the three (IOF, ITF and IL) bearing loads. The test setups of the IOF, ITF and IL conditions are illustrated in Figure. 2. The details of the testing procedures are described in Cai and Young [23]. It should be noted that design rules of flanges fastened or unfastened to the supports are given in the specifications [19-21,24]. The flanges of the CFLDSS specimens were not fastened to the steel bearing plates in the test program [23] and in the study of the present paper. This is because the flanges of steel tubular members may not be easy to fasten in practice, e.g., tubular sections that located at multiple span of floor joists.

Two different grades of CFLDSS (i.e., EN 1.4062 and EN 1.4162) were considered. Their material properties were measured by conducting tensile and compressive coupon tests. The tensile coupons were extracted in the longitudinal direction of the members, and the compressive coupons were cut from the transverse direction of the webs. Table 1(a) shows the Young's modulus (E_T and E_C), 0.2% proof stress ($f_{0.2,T}$ and $f_{0.2,C}$) and strain at fracture ($\varepsilon_{f,T}$) of the CFLDSS tubular members, where the results from tensile and compressive tests were distinguished by the subscripts "T" and "C", respectively.

Figure 1 illustrates the definition of the symbols in a CFLDSS section, where H and h are the over height and the flat portion of the section web, respectively; B is for the section width, t for section thickness and r_i for inner radius. Totally fifty-three CFLDSS specimens were tested [23]. These covered nine tubular sections (H×B×t), three loading conditions (IOF, ITF and IL), six bearing lengths (N) as well as a range of h/t and the ratio of inner corner radius (r_i) to tube thickness (t). Tables 2-4 illustrate the test specimens and test strengths (P_t) of CFLDSS specimens per web for IOF, ITF and IL conditions, respectively. Each specimen was identified by a label starting with the interior loading condition (IOF, ITF or IL), followed by the cross-section nominal dimension (H×B×t in mm) and the loaded bearing length (N), for example, Specimen IOF100×100×3.0N90. In some cases, the last segment "-r" in the label indicates that it is a repeated test specimen. The details of test setups and testing procedures are described in Cai and Young [23].

3. Finite element models

3.1. General

The ABAQUS program of version 6.20 [34] was adopted in the development of the finite element models (FEMs) to simulate the web crippling tests of CFLDSS specimens. The accuracy of the FEMs were assessed by comparing the FE results with the test results, including the failure modes, ultimate strengths and load-deformation curves.

3.2. Element types and element sizes

Shell element type S4R that is a four-node doubly curved element with reduced integration and hourglass control was selected to simulate the CFLDSS tubular specimens. The element S4R has been adopted [31,32] in the successful simulation on the behaviour of ferritic stainless steel tubular members undergoing web crippling. The solid element type C3D8R was selected to simulate the steel bearing plates. The bearing plates were defined as rigid body as the steel bearing plates in the test program [23] were fabricated by high strength steel which had much higher yield strength than those of the CFLDSS specimens. The mesh sizes were varied in the range of 2×2 mm to 10×10 mm (length by width) for the flat portions of the web that depending on the dimension of the web. Similar mesh sizes were adopted based on the sensitivity study by Li and Young [31,32] for ferritic stainless steel tubular members subjected to the same loading conditions as those in this study. Finer mesh size with five elements was generally employed for the corner radius of the section.

3.3. Material properties

The measured engineering stress-strain curves were converted to true plastic stress-strain curves before inputting in the FEMs. Due to the effect of cold working, the CFLDSS tubular sections at corner regions were strengthened. It had higher 0.2% proof stress and ultimate strength than those at the flat regions. Hence, the material properties at the corner regions were also considered in this study. The corner material properties were measured by the longitudinal corner coupon tests [35,36]. The material properties of CFLDSS tubular members investigated by Xing and Young [35] as well as Wang *et al.* [36] had the same section dimensions and also belonged to the same batch of CFLDSS tubes as those of the test specimens [23]. The measured Young's modulus (E_T), 0.2% proof stress ($f_{0.2,T}$) and strain at fracture ($\varepsilon_{f,T}$) of the longitudinal corner coupons are tabulated in Table 1(b).

The corner material properties were assigned to the region of curved corners with the extension of twice the section thickness (2*t*) to adjacent flat regions [31,32]. The tensile flat material properties (see Table 1(a)) [23] were assigned to the flanges of the sections. In this study, two different cases of material properties were considered at the flat web portions (*h*-2*t*) of the sections. In the first case, the same tensile material properties [23] as those for the flanges were used; while in the second case, the compressive material properties (see Table 1(a)) [23] that obtained in the transverse direction of the webs were used. Hence, the effects of tensile and compressive material properties that assigned to the webs of the sections were investigated.

3.4. Boundary conditions

The boundary conditions of the test setups were symmetric [23]. Hence, symmetric boundary conditions were considered in the FEMs (e.g., the model for IOF loading condition in Figure 2). Contact pairs were assigned in the simulation of the interfaces between the steel bearing plates and the stainless steel specimens. In each contact pair, master surface and slave surface were defined. The steel bearing plate was defined as master surface, whereas the test specimen was defined as slave surface. The rounded corners of the section that initially un-contacted with the steel bearing plates may gradually become contacted due to the large deformations as applied load increased. Hence, the section corners adjacent to the flanges were also defined in the slave surfaces. The "Hard Contact" was defined in the normal direction while a coefficient of 0.4 was considered for the friction penalty contact in the tangential direction [31,32].

It should be noted that for the tests under IOF loading condition, steel stiffening plates at end supports were used to prevent web failure [23]. Similarly, the flat webs at both end supports in the FEM were restrained (U_x = 0, where U_x means translation in X direction) by the same length as the steel stiffening plates (see Figure 3**)**. Proper boundary conditions were assigned to the reference points of the steel bearing plates to simulate the roller support and half round support in the test setup. For example, the boundary conditions of $U_x = 0$, $U_z = 0$, $R_y = 0$ and $R_z = 0$ (R_y and R_z mean the rotation about direction in Y and Z axes, respectively) were assigned to RP-1 (see Figure 3**)** of the bearing plate to simulate the half round support.

The initial geometrical imperfection of the web was not considered in the FEMs, as previous numerical studies by Natário *et al.* [37] found that the initial geometrical imperfection had barely perceptible effect on the load-displacement curve of the lipped channel section undergoing web crippling. The NLGEOM commend is activated in order to consider the geometrical nonlinearity of the FE model [34]. An axial displacement was specified to the reference point in the FEM. This was identical to the test program where the loads were applied by displacement control [23]. The comparison of the tests and FEMs for CFLDSS specimens subjected to different loading conditions are illustrated in Figures 4-6, for specimens of IOF100×100×3.0N90, ITF120×60×3.0N30 and IL150×80×3.0N30, respectively.

4. Validation of FEMs

The FE ultimate strengths (P_{FEA}) per web predicted by the FE analysis were compared with the test strengths (P_t) per web obtained from the experimental program [23], as shown in Tables 2-4. As mentioned previously, for the flat web portions, there were two cases of material properties considered in the FEMs. The first case used the longitudinal tensile material properties and the second case used the transverse compressive material properties. The FEA predictions obtained from the first and second cases were indicated by $P_{FEA\text{-}1}$ and $P_{FEA\text{-}2}$, respectively.

For the first case, the average values of the $P_t/P_{FEA\text{-}1}$ are 1.01, 0.98 and 1.00 for the IOF, ITF and IL conditions, respectively, with the corresponding coefficients of variation (COVs) of 0.064, 0.054 and 0.073; while for the second case, the average values of $P_t/P_{FEA\text{-}2}$ are 0.99, 0.96 and 0.97 with their respective COVs of 0.072, 0.072 and 0.083 (see Tables 2-4). Table 5 further summarizes the overall comparisons of test strength-to-FEA predictions. It is shown that the mean values of the $P_t/P_{FEA\text{-}1}$ and $P_t/P_{FEA\text{-}2}$ are 0.99 and 0.97 with the corresponding COVs of 0.064 and 0.076. Overall, the two cases of using different material properties in the flat webs are capable to predict the test strengths. However, the first case provides slightly better predictions with the mean value of 0.99 and slightly smaller value of COV than the second case, where the corner material properties [35,36] in the corners of the sections, longitudinal tensile material properties [23] in the flat portion of webs and flanges of the sections were used. The comparison of failure mode for specimens of IOF150×80×3.0N30, ITF80×150×3.0N60 and IL150×80×3.0N30 are shown in Figures 7-9, respectively. Figure 10 illustrates the comparison of the load-web deformation curves between the tests and FEA predictions, including the specimens IOF150×80×3.0N90 and ITF100×100×3.0N90.

5. Parametric study

It is shown from the FEA predictions, that using the longitudinal tensile flat coupons [23] and longitudinal tensile corner coupons [35,36], are capable to replicate the behaviour of CFLDSS tubular members subjected to the concentrated IOF, ITF and IL conditions. Hence, after the successful validation, the FEMs were employed to perform a parametric study on CFLDSS tubular members under the three interior loading conditions. The key parameters in the web crippling design of CFLDSS members were considered carefully. These included the h/t, N/t, N/h and r_i.

The dimensions (H×B×t) of the cross-sections and the key parameters are tabulated in Table 6. In total, 24 hollow sections were considered in this study. The dimensions of the cross-sections ranged from 60×60×1.5 mm to 400×200×8 mm. The ratio of r_i/t for each specimen, was designed based on the handbook provided by the test specimen supplier. The radio of r_i/t either equal to 1.0 or 1.5 was used, as shown in Table 6. Hence, the variation of r_i was achieved by different values of t. Each section was loaded with two different bearing lengths (N), i.e., either N = 0.5B or N = 1.0B in each loading condition (IOF, ITF or IL). Hence, the varied parameters of h/t, N/t and N/h were obtained, and they were ranged from 11.0 to 145.0, 7.5 to

150.0 and 0.26 to 1.36, respectively (see Table 6). The design of specimen length is identical to those adopted in the test program [23]. In addition, same criteria as those in the test program [23], the distance of 1.5H was designed for the clear distance of the two adjacent bearing plate edges in the IOF loading condition; and the 1.5H clear distance was adopted between the specimen free end and the adjacent bearing plate edge for the ITF and IL conditions.

The material properties of section 100×100×3.0 [23,36] were used in the parametric study. Note that the curved corners of the sections were assigned by the corner material properties. In total, 144 specimens were analysed for the web crippling of CFLDSS tubular members under the three interior loading conditions. The FE ultimate strengths (P_{FEA}) of the specimens per web are tabulated in Tables 7-9 for the IOF, ITF and IL conditions, respectively.

6. Reliability analysis

Reliability analysis was performed by following the method in the Section 6.2 of the ASCE Specification [19]. In this study, the design provisions were considered as probabilistically safe and reliable provided that the value of the reliability index (β) satisfied $\beta \geq 2.5$. In the calculation of β, the load combinations of 1.2DL + 1.6LL (DL = dead load, LL = live load) was used for the design provisions of ASCE [19], NAS [24], Zhou and Young [25] and the modified DSM [31,32], while the 1.35DL + 1.5LL specified in the European code [38] was considered for the EC3-1.4 predictions [21]. The DL/LL was set as 0.2 [19]. The suggested mean values and COVs of the material factor are M_m = 1.10 and F_m = 1.00, respectively; and those of fabrication factor are V_M = 0.10 and V_F = 0.05 in Section 6.2 of ASCE [19]. In addition, the effects of limited test and numerical results were considered by using a correction factor (C_P) [19]. The reliability analyse results will be discussed in the later sections of this paper.

7. Current design rules and assessments

7.1. General

The web crippling design rules for stainless steel members [19-21] were used to calculate the nominal web crippling strengths per web of the CFLDSS tubular members under the three loading conditions. The design rules in the ASCE [19] and the AS/NZS [20] are identical. Hence, they provide identical strength predictions. Since web crippling design rules are not provided in the EC3-1.4 [21], hence, in the strength calculations predicted by Eurocode, those specified in the EC3-1.3 [39] for cold-formed steel members, where the design for “Local transverse forces” in Section 6.1.7.3 of the EC3-1.3 [39] was used. Apart from the aforementioned stainless steel design specifications, the unified design equation specified in the NAS [24] for different concentrated loading conditions was also adopted and assessed in this study, even though it is not specified for stainless steel members. The design rules found in the literature were also used and assessed, including the modified unified design equation for duplex stainless steel [25], and the direct strength method (DSM) for ferritic stainless steel [31,32]. It should be noted that the design of CFLDSS members is not covered in these design rules.

7.2. Design specifications

The differences of the current codified design rules [19-21] are discussed in detail by Cai and Young [23], including those specified in Section 3.3.4 of the ASCE [19], in Section 6.1.7.3 of the EC3-1.3 [39], and in Section G5 of the NAS [24]. The unified design equation specified in NAS [24] is illustrated in Equation (1). This unified web crippling equation was firstly developed by Prabakaran [40] and Prabakaran and Schuster [41] for different geometric shapes and loading conditions, including the IOF and ITF in this study. The equation was extended to cover other geometric shapes of carbon steel members by Behsara and Schuster [42], and other materials, e.g., austenitic and duplex stainless steel by Zhou and Young [25].

$$P = Ct^2 f_{0.2} \sin\theta \left(1 - C_R\sqrt{\frac{r_i}{t}}\right)\left(1 + C_N\sqrt{\frac{N}{t}}\right)\left(1 - C_h\sqrt{\frac{h}{t}}\right) \quad (1)$$

where P standards for the nominal web crippling strength per web, the coefficients of C, C_R, C_N, C_h represent the coefficient of overall web crippling, inside corner radius, bearing length and the web slenderness, respectively. The coefficients and the application limits specified in NAS [24] for Eq. (1) are shown in Table 10.

The ASCE [19] and NAS [24] specifications provide the design rules for IOF and ITF loading conditions. However, the IL condition is not specified in these two specifications. For the purpose of assessment, the design for IOF and ITF loading conditions in ASCE [19] and NAS [24] were both used for the strength predictions of the IL condition.

7.3. Unified design equation and modified DSM in literature

The aforementioned unified design equation (Eq. (1)) in NAS [24] has been modified by Zhou and Young [25] for the web crippling design of cold-formed duplex stainless steel members under different loading conditions. Different sets of coefficients were proposed for different loading conditions [25], as shown in Table 10.

The Direct Strength Method (DSM) has been developed for design of cold-formed steel structural members. However, the DSM in current NAS [24] does not provide design rules for cold-formed steel tubular members undergoing web crippling. Investigations of DSM for the web crippling design of cold-formed steel open sections were conducted by Keerthan *et al*. [43] and Natário *et al*. [44,45]. Recently, Li and Young [31,32] extended the DSM to cover the web crippling design of cold-formed ferritic stainless steel tubular members, as illustrated in Eq. (2). Different sets of coefficients were proposed [31,32] for different loading conditions.

$$P_{DSM} = \begin{cases} \gamma P_y & \lambda \le \lambda_k \\ a\left[1 - b\left(\frac{P_{cr}}{P_y}\right)^n\right]\left(\frac{P_{cr}}{P_y}\right)^n P_y & \lambda > \lambda_k \end{cases} \tag{2}$$

where $\lambda = \sqrt{P_y/P_{cr}}$ is the web crippling slenderness ratio. The P_{cr} and P_y are the nominal bearing strengths per web for buckling and yielding, respectively, as refer to the Clause 5.13 of the AS4100 [46]. The coefficients of a, b, n, γ and λ_k proposed by Li and Young [31,32] for cold-formed ferritic stainless steel tubular members under different interior loading conditions are tabulated in Table 11. The λ_k indicates the cross point of the DSM curve, where the lower bound (conservative manner) of strength predictions are generally adopted for tubular sections with lower values of web crippling slenderness ratio.

The DSM generally requires aid from computer software for the determination of P_{cr} [44,45]. As an alternative, the calculations of P_{cr} could be done manually by Eqs. (3)-(7) as specified in the AS4100 [46]:

$$P_{cr} = \alpha_c t N_m f_{0.2} \tag{3}$$

where α_c is the slenderness reduction factor with the calculation procedures as detailed in Clause 6.3.3 of AS4100 [46], and N_m is the mechanism length determined by Eq. (4),

$$N_m = N + 5R + h \tag{4}$$

where R is the outer corner radius. Eq. (4) is applicable for the CFLDSS tubular members subjected to the IOF, ITF and IL conditions.

$$P_y = \alpha_p t N_m f_{0.2} \tag{5}$$

The Clause 5.13 of AS4100 [46] categorized different loading conditions into end bearing and interior bearing only. For interior loading conditions:

$$\alpha_p = \frac{0.5}{k_s}\left[1 + \left(1 - \alpha_{pm}^2\right)\left(1 + \frac{k_s}{k_v} - \left(1 - \alpha_{pm}^2\right)\frac{0.25}{k_v^2}\right)\right] \tag{6}$$

While for end loading conditions:

$$\alpha_p = \sqrt{2 + k_s^2} - k_s \tag{7}$$

where $k_s = 2R/t-1$, $\alpha_{pm} = 1/k_s + 0.5/k_v$ and $k_v = h/t$.

It should be noted that α_p in Eq. (7) was used by Li and Young [32] for ITF loading condition.

7.4. Assessment of current design predictions

The aforementioned design rules were assessed by comparing the predicted strengths with those obtained from the tests and parametric study, as shown in Tables 7-9 for the IOF, ITF and IL conditions, respectively. The ultimate strengths (P_u) per web represent the strengths either obtained from the tests (P_t) or FEA (P_{FEA}). The predicted strengths for the test specimens were calculated using the measured dimensions and the corresponding tensile material properties (see Table 1), whereas the predicted strengths for the FEA specimens were calculated using the nominal dimensions and the tensile material properties (see Table 1 for Section 100×100×3.0).

For the predictions by ASCE [19], the mean values of P_u/P_{ASCE} are 1.17, 1.11, 1.36 (1.23), with the corresponding COVs of 0.120, 0.181 and 0.150 (0.227), for the loading conditions of IOF, ITF and IL, respectively. Note that the designs for IOF (ITF) were used for the condition of IL. The predictions by ASCE [19] are overall conservative as all the mean values are larger than 1.00. While the predictions by EC3-1.3 [39] for the IOF, ITF and IL, the mean values of P_u/P_{EC} are 2.91, 6.09 and 3.34, respectively, with the corresponding COVs of 0.174, 0.145 and 0.182. Overall, the predictions by EC3-1.3 [39] are much more conservative than those predicted by ASCE [19]. This is mainly due to the ratio of h/t and the N are not considered in the design provisions [39]. However, these key parameters are considered in other design provisions [19,24,25]. Note that the CFLDSS specimen sections had different web slenderness (h/t) and were loaded by steel plates with different bearing lengths (N) in the range of 30 to 300 mm in this study. However, the EC3-1.3 [39] uses the same bearing length of 10 mm in calculating the design predictions. The conservative predictions by EC3-1.3 [39] were also discussed and explained in Cai and Young [22,23].

For the predictions by using the unified design equation (Eq. (1)) in NAS [24], the mean values of the P_u/P_{NAS} are 0.92, 0.85, 1.04 (0.92), with the corresponding COVs of 0.095, 0.201 and 0.099 (0.179), for the loading conditions of IOF, ITF and IL, respectively. Similar to the comparisons for ASCE [19], the designs for IOF (ITF) were used for the IL condition, where it shows that overall, the mean value obtained from IOF is closer to 1.00 (1.04 compared with 0.92) and the predictions are less scattered. While for the predictions by using the modified coefficients proposed in [25], the mean values of $P_u/P_{Z\&Y}$ are 1.14, 1.09 and 1.09, with the corresponding COVs of 0.070, 0.125 and 0.118, for the loading conditions of IOF, ITF and IL, respectively. Overall, the predictions are conservative.

By using the design of DSM [31,32], the mean values of $P_u/P_{L\&Y}$ are 1.17, 1.12 and 1.09 for the IOF, ITF and IL, respectively, with the corresponding COVs of 0.077, 0.104 and 0.118. The predictions are also overall conservative. However, it was found that the DSM [31,32] provided less scattered predictions than the codified predictions by ASCE [19], EC3-1.3 [39] and NAS [24], as the COV is the smallest in the comparisons for the three interior loading conditions (see Tables 7-9).

The comparisons of the ultimate strengths (P_u) per web with the aforementioned predictions are shown in Figures 11-15. The comparisons were plotted against the values of h/t, i.e., web slenderness ratio. Generally, the predictions by ASCE [19] are more conservative for the larger values of h/t, i.e., more slender webs, for both IOF and ITF conditions (see Figure 11). The NAS [24] generally provides un-conservative predictions for both the IOF and ITF regardless of different values of h/t (see Figure 12). Note that for the IL condition, the superscripts of "#" and "*" indicate that the predictions were calculated by using the design rules for IOF and ITF, respectively (see Figures 11-12). The EC3-1.3 [39] provides more conservative predictions for the ITF than those for the IOF and IL conditions under different values of h/t (see Figure 13). The predictions by Zhou and Young [25] generally become unconservative for the higher values of h/t (h/t > 75) for ITF loading condition, as shown in Figure 14. Overall, the predictions provided by Li and Young [31,32] are conservative. However, the predictions are unconservative for very slender webs, i.e. h/t = 145, for ITF and IL conditions (see Figure 15).

Reliability of these design provisions was assessed by adopting the reliability analysis specified in Section 5 of the present paper. The recommended resistance factors (ϕ) for the corresponding design rules [19,21,24,25,31,32] (see Tables 7-9) were used for the calculation of reliability index (β). It was found that all the current design provisions for the IOF and ITF are probabilistically safe and reliable (β > 2.50), except for the NAS predictions [24] with β =

2.07 for IOF and β = 1.82 for ITF which are smaller than the target value of 2.50 (see Tables 7-8). The current design provisions for the IL condition are also probabilistically safe and reliable, except for NAS [24] due to the β = 2.17 when using the coefficients for ITF [24], as shown in Table 9.

8. Proposed design rules and assessments

8.1. General

As discussed in Section 7.4 of this paper, the predictions by the ASCE [19], EC3-1.3 [39], the modified unified design equation [25] and the modified DSM (Eq. (2)) [31,32] are generally conservative and reliable, in particular, very conservative predictions by EC3-1.3 [38]. The predictions by the original unified design equation in NAS [24] are generally not reliable. Hence, efforts were made for the improvements of the web crippling design (for Eq. (1) and Eq. (2)) of CFLDSS tubular members in this study.

8.2. Modified coefficients for unified design equation

Three new sets of coefficients are proposed for IOF, ITF and IL conditions for the original unified design equation Eq. (1) in NAS [24]. The coefficients were calibrated against both the 58 test results [23] and the 144 parametric results obtained in this study. The new coefficients for Eq. (1) are reported in Table 10, including C, C_R, C_N, and C_h. The overall web crippling coefficient, C = 8.0, C = 8.3 and C = 9.1 are proposed for the IOF, ITF and IL conditions, respectively. Note that different values of coefficients (C_R, C_N and C_h) are specified in NAS [24] and Zhou and Young [25] for different loading conditions. However, constant coefficients of C_R = 0.21, C_N = 0.26 and C_h = 0.001 are proposed in this study for CFLDSS square and rectangular hollow sections, as shown in Table 10. In addition, a constant value of resistance factor of ϕ = 0.85 is proposed for the three loading conditions. The value of 0.85 is larger than those proposed by Zhou and Young [25] for different loading conditions. These proposed coefficients for Eq. (1) are applicable for web crippling deign of CFLDSS square and rectangular hollow sections. The flanges of these sections are stiffened or partially stiffened. The application limits are $10 \leq h/t \leq 145$, $r_i/t \leq 2.0$, $N/t \leq 150$ and $N/h \leq 1.5$.

8.3. Modified direct strength method

It has been shown that the modified DSM design equation (Eq. (2)) generally provided conservative predictions, in particular for the loading conditions of IOF and ITF. Hence, improvements on the modified DSM design equation (Eq. (2)) were made by proposing three new sets of coefficients for IOF, ITF and IL conditions. The coefficients were also calibrated against both the test results and numerical results. The new coefficients of a, b, n, λ_k, and γ for Eq. (2) are reported in Table 11. Similar to those suggested by Li and Young [31,32], different values of a, λ_k and γ are proposed for different loading conditions. However, the constant coefficients of n = 0.35 and λ_k = 0.60 are proposed regardless of different interior loading conditions. For consistence in the determination of α_p for interior loadings, the Eq. (6) for interior bearing loads was used for the three different loading conditions in the present study. These proposed coefficients (see Table 11**)** for Eq. (2) are applicable for CFLDSS square and rectangular hollow sections. The flanges of these sections are stiffened or partially stiffened. The application limits are $10 \leq h/t \leq 145$, $r_i/t \leq 2.0$, $N/t \leq 150$ and $N/h \leq 1.5$.

8.4. Assessment of modified design predictions

The modified design rules were assessed by comparing the predicted strengths with those obtained from the tests and parametric study. The predicted strengths were calculated by Eq. (1) and Eq. (2) using the newly proposed coefficients (see Tables 10-11), and these predictions were represented by P_1 and P_2, respectively. In the calculations, the material properties were used in the same criteria as those described in Section 7.4 of this paper.

Using Eq. (1) for the IOF, ITF and IL conditions, the mean values of the P_u/P_1 are 0.99, 1.01 and 1.00, respectively, with the corresponding COVs of 0.070, 0.117 and 0.097. The predictions by Eq. (1) using the newly proposed coefficients are probabilistically safe and reliable as all the values of β are larger than 2.50. Figure 16 illustrates the comparison of P_u and P_1 for the three interior loadings.

Using Eq. (2) for the IOF, ITF and IL conditions, the mean values of the P_u/P_2 are 0.99, 1.07 and 1.07, respectively, with the corresponding COVs of 0.086, 0.104 and 0.073. The predictions by Eq. (2) using the proposed new coefficients are all probabilistically safe and reliable (β > 2.5). Figure 17 illustrates the comparison of P_u and P_2 for the three interior loadings. Furthermore, Figures 18-20 show the DSM curves and the test and numerical results for the IOF, ITF and IL conditions, respectively. In each figure, the ratio of P_u/P_y were plotted against the ratio of $(P_y/P_{cr})^{0.5}$. Generally, it is shown that the modified DSM curves in this study provide better fitting than the DSM curves proposed by Li and Young [31,32].

9. Conclusions

Non-linear finite element models (FEMs) have been developed for web crippling of cold-formed lean duplex stainless steel (CFLDSS) tubular members. The tubular members were loaded under three interior loading conditions, namely, the interior-one-flange (IOF), interior-two-flange (ITF) and interior loading (IL). The accuracy of the FEMs were assessed in terms of the predicted ultimate strengths, failure modes and load-deformation curves. An extensive parametric study of 144 CFLDSS specimens under the three interior loadings was performed by using the verified FEMs. The key parameters were considered in the parametric study. The key parameters cover the ratios of flat web height to thickness, bearing length to web thickness and bearing length to flat web height, as well as the inner corner radius of the sections.

The accuracy and reliability were assessed for the current design rules in the international specifications of the ASCE [19], AS/NZS [20], EC3 [21,39] and NAS [24], as well as those in the literature, namely, the modified unified equation [25] and the modified direct strength method (DSM) [31,32]. It was found that the predictions by the current codified design rules [19-21,39] and those in the literature [25,31,32] are generally conservative and reliable. However, the NAS [24] generally provided unconservative and not reliable predictions.

New sets of coefficients are proposed for the unified design equation and the modified DSM. The proposed coefficients were calibrated against both the test results and numerical results. By using the newly proposed coefficients in the design calculations, it is shown that the predictions by the unified equation and the modified DSM are more accurate than those aforementioned predictions, and the predictions are also probabilistically safe and reliable. Therefore, the newly proposed coefficients for the unified equation and the modified DSM are suggested for the web crippling design of CFLDSS tubular members with square and rectangular hollow sections under the three interior (i.e., IOF, ITF and IL) loading conditions. The flanges of the members are stiffened or partially stiffened that unfastened to the supports. The application limits are $10 \leq h/t \leq 145$, $r_i/t \leq 2.0$, $N/t \leq 150$ and $N/h \leq 1.5$.

Acknowledgement

The authors wish to acknowledge the support provided by the Chinese National Engineering Research Centre for Steel Construction (Hong Kong Branch) at the Hong Kong Polytechnic University which is funded by the Innovation and Technology Fund administrated by the Innovation and Technology Commission of the Commissioner of the Government of Hong Kong SAR.

References

[1] Zhou, F. and Young, B. Experimental and numerical investigations of cold-formed stainless steel tubular sections subjected to concentrated bearing load. Journal of Constructional Steel Research 2007, 63(11): 1452-1466.

[2] Young, B. Hancock, G. J. Design of cold-formed channels subjected to web crippling. Journal of Structural Engineering 2001, 127(10): 1137-1034.

[3] Gardner, L. and Baddoo, N.R. Fire testing and design of stainless steel structures. Journal of Constructional Steel Research 2006, 62(6): 532–543.

[4] Huang, Y. and Young, B. Material properties of cold-formed lean duplex stainless steel sections. Thin-Walled Structures 2012, 54: 72-81.

[5] Theofanous, M. and Gardner L. Testing and numerical modelling of lean duplex stainless steel hollow section columns. Engineering Structures 2009, 31: 3047-3058.

[6] Saliba, N. and Gardner, L. Cross-section stability of lean duplex stainless steel welded I-sections. Journal of Constructional Steel Research 2013, 18: 1-14.

[7] Huang, Y. and Young, B. Experimental and numerical investigation of cold-formed lean duplex stainless steel flexural members. Thin-Walled Structures 2014, 73: 216-228.

[8] Zhao, O., Afshan, S. and Gardner, L. Structural response and continuous strength method design of slender stainless steel cross-sections. Engineering Structures 2017, 140, 14-25.

[9] Zhao, O. and Gardner, L. The continuous strength method for the design of mono-symmetric and asymmetric stainless steel cross-sections in bending. Journal of Constructional Steel Research 2018, 150, 141-152.

[10] Huang, Y. and Young, B. Tests of pin-ended cold-formed lean duplex stainless steel columns. Journal of Constructional Steel Research 2013, 82: 203-215.

[11] Zhao, O., Rossi, B., Gardner, L. and Young, B. Behaviour of structural stainless steel cross-sections under combined loading – Part I: Experimental study. Engineering Structures 2015, 89, 236-246.

[12] Zhao, O., Rossi, B., Gardner, L. and Young, B. Behaviour of structural stainless steel cross-sections under combined loading – Part II: Numerical modelling and design. Engineering Structures 2015, 89, 247-259.

[13] Saliba, N. and Gardner L. Experimental study of the shear response of lean duplex stainless steel plate girders. Engineering Structures 2013, 46: 375-391.

[14] Saliba N., Real, E., Gardner, L. Shear design recommendations for stainless steel plate girders. Engineering Structures 2014, 59: 220-228.

[15] Cai, Y. and Young, B. Structural behavior of cold-formed stainless steel bolted connections. Thin-Walled Structures 2014, 83: 147-156.

[16] Cai, Y. and Young, B. Behavior of cold-formed stainless steel single shear bolted connections at elevated temperatures. Thin-Walled Structures 2014, 75: 63-75.

[17] Cai, Y. and Young, B. Transient state tests of cold-formed stainless steel single shear bolted connections. Engineering Structures 2014, 81: 1-9.

[18] Cai, Y. and Young, B. High temperature tests of cold-formed stainless steel double shear bolted connections. Journal of Constructional Steel Research 2015, 104: 49-63.

[19] ASCE. Specification for the design of cold-formed stainless steel structural members. American Society of Civil Engineers (ASCE), ASCE Standard, SEI/ASCE-8-02, Reston, Virginia, 2002.

[20] AS/NZS. Cold-formed stainless steel structures. AS/NZS 4673:2001, Australian/New Zealand Standard (AS/NZS), Standards Australia, Sydney, Australia, 2001.

[21] EC3-1.4. Eurocode 3. Design of steel structures - Part 1.4: General rules - Supplementary rules for stainless steels. EN 1993-1-4:2006+A1:2015, Brussels, Belgium, European Committee for Standardization, 2015.

[22] Cai, Y. and Young, B. Web crippling of lean duplex stainless steel tubular sections under concentrated end bearing loads. Thin-Walled Structures 2019, 134: 29-39.

[23] Cai, Y. and Young, B. Cold-formed lean duplex stainless steel tubular members under concentrated interior bearing loads. Journal of Structural Engineering 2019, ASCE. 145(7): 04019056.

[24] North American Specification (NAS). North American Specification for the design of cold-formed steel structural members. AISI S100–16, Washington D. C., USA: American Iron and Steel Institute (AISI); 2016.

[25] Zhou, F. and Young, B. Web crippling of cold-formed stainless steel tubular sections. Advances in Structural engineering 2008, Vol. 11, No. 6, 679-691.

[26] Gardner, L., Talja, A. and Baddoo, N.R. Structural design of high-strength austenitic stainless steel. Thin-Walled Structures 2006, 44: 517-528.

[27] Zhou, F. and Young, B. Cold-formed stainless steel sections subjected to web crippling. Journal of Structural Engineering 2006, 132(1): 134-144.

[28] dos Santos, G.B., Gardner L. and Kucukler M. Experimental and numerical study of stainless steel I-sections under concentrated internal one-flange and internal two-flange loading Engineering Structures 2018, 175: 355-370.

[29] dos Santos, G.B. and Gardner L. Testing and numerical analysis of stainless steel I-sections under concentrated end-one-flange loading. Journal of Constructional Steel Research 2019, 157: 271-281.

[30] Bock, M., Arrayago, I., Real, E. and Mirambell, E. Study of web crippling in ferritic stainless steel cold formed sections. Thin-Walled Structures 2013, 69: 29-44.

[31] Li, H-T. and Young, B. Cold-formed ferritic stainless steel tubular structural members subjected to concentrated bearing loads. Engineering Structures 2017, 145: 392-405.

[32] Li, H-T. and Young, B. Web crippling of cold-formed ferritic stainless steel square and rectangular hollow sections. Engineering Structures 2018, 176: 968-980.

[33] Zhou, F. and Young, B. Cold-formed high-strength stainless steel tubular sections subjected to web crippling. Journal of Structural Engineering 2007, 133(3): 368-377.

[34] ABAQUS Analysis User's Manual, ABAQUS, Inc., Version 6.20, 2019.

[35] Xing, B. and Young, B. Experiental investigation of concrete-filled lean duplex stainless steel RHS stub columns. Proceedings of 16th International Symposium on Tubular Structures (ISTS16) 2017, Eds. Heidarpour A. and ZHAO X.-L. Melbourne, Australia. 95-100.

[36] Wang, F., Young, B. and Gardner, L. Experimental Study of Square and Rectangular CFDST Sections with Stainless Steel Outer Tubes under Axial Compression. Journal of Structural Engineering 2019, ASCE, 145(11): 04019139.

[37] Natário, P., Silvestre, N. and Camotim, D. Web crippling failure using quasi-static FE models. Thin-Walled Structures 2014, 84, 34-49.

[38] EC0. Eurocode 0: basis of structural design. EN 1990:2002+A1:2005. Brussels, Belgium: European committee for standardization; 2005.

[39] EC3-1.3. Eurocode 3: Design of steel structures - Part 1–3: General rules – Supplementary rules for cold-formed members and sheeting. EN 1993-1-3, Brussels, Belgium: European committee for standardization; 2006.

[40] Prabakaran, K. (1993). Web Crippling of Cold Formed Steel Sections, Project Report, Department of Civil Engineering, University of Waterloo, Waterloo, Ontario, Canada, April.

[41] Prabakaran, K., and Schuster, P.M. (1998). "Web crippling of cold-formed steel members." Proceedings of the 14th International Specialty Conference on Cold formed Steel Structures, St. Louis, University of Missouri-Rolla, Mo., 151-164.

[42] Beshara, B., and Schuster, P.M. (2000). “Web crippling data and calibrations of cold formed steel members.” Final Report, University of Waterloo, Waterloo, Canada.

[43] Keerthan P, Mahendran M, Steau E. Experimental study of web crippling behaviour of hollow flange channel beams under two flange load cases. Thin-Walled Structure 2014; 85:207-19.

[44] Natário P, Silvestre N, Camotim D. Web crippling of beams under ITF loading: a novel DSM-based design approach. Journal of Constructional Steel Research 2017; 128:812-24.

[45] Natário P, Silvestre N, Camotim D. Direct strength prediction of web crippling failure of eams under ETF loading. Thin-Walled Structure 2016; 98:360-74.

[46] Australian Standard (AS). Steel structures. AS 4100, Sydney, Australia: Standards Australia; 1998.

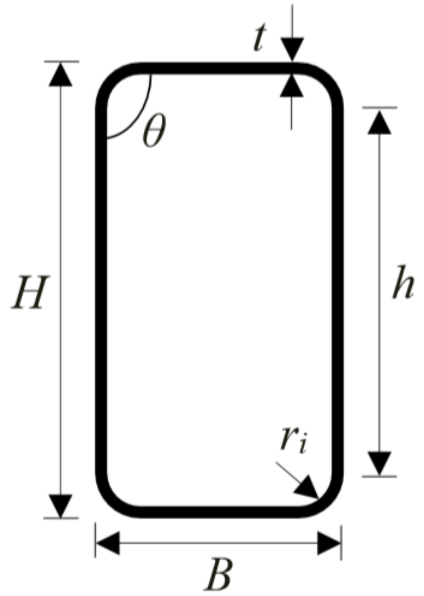

Figure 1: Definition of symbols in a tubular section

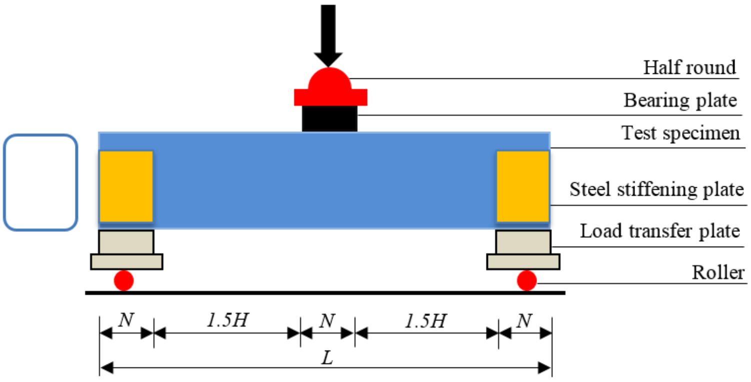

(a) Interior-One-Flange (IOF) loading condition

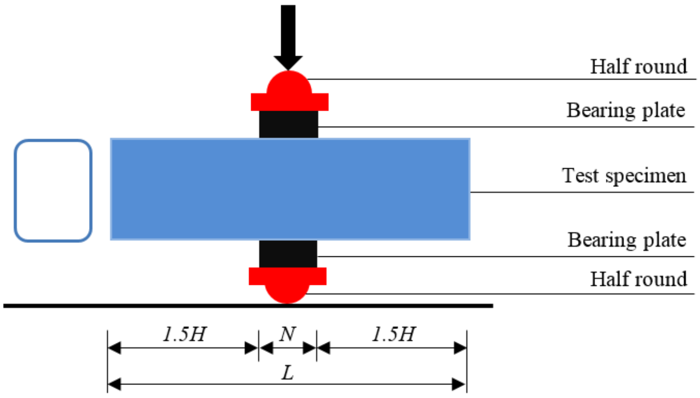

(b) Interior-Two-Flange (ITF) loading condition

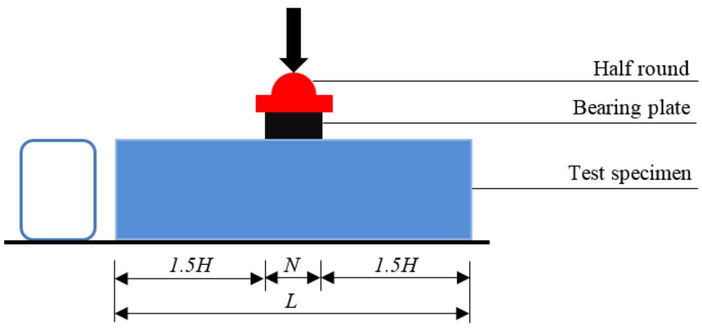

(c) Interior loading (IL) condition

Figure 2: LDSS specimens under different concentrated interior bearing loads [23]

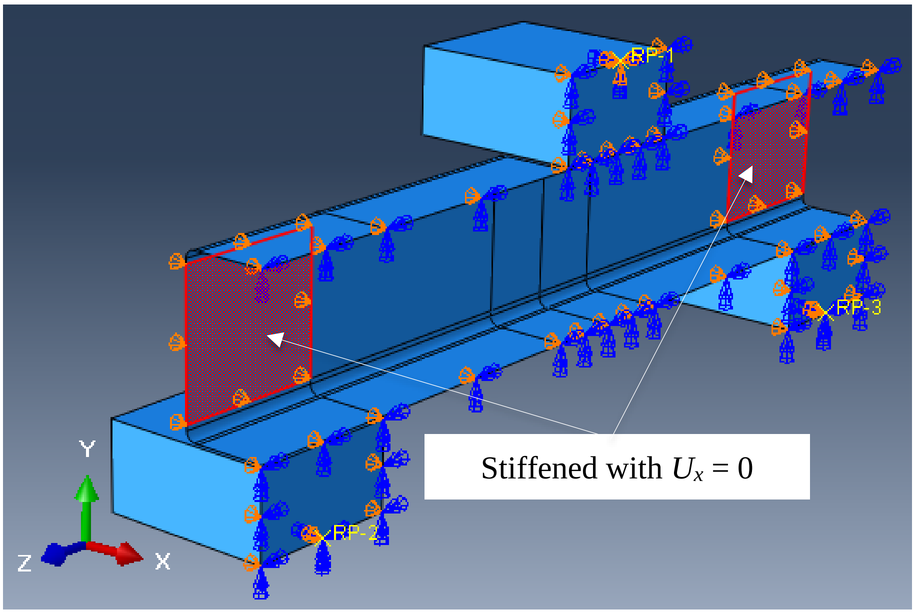

Figure 3: Symmetric finite element model (FEM) for specimen under IOF loading condition

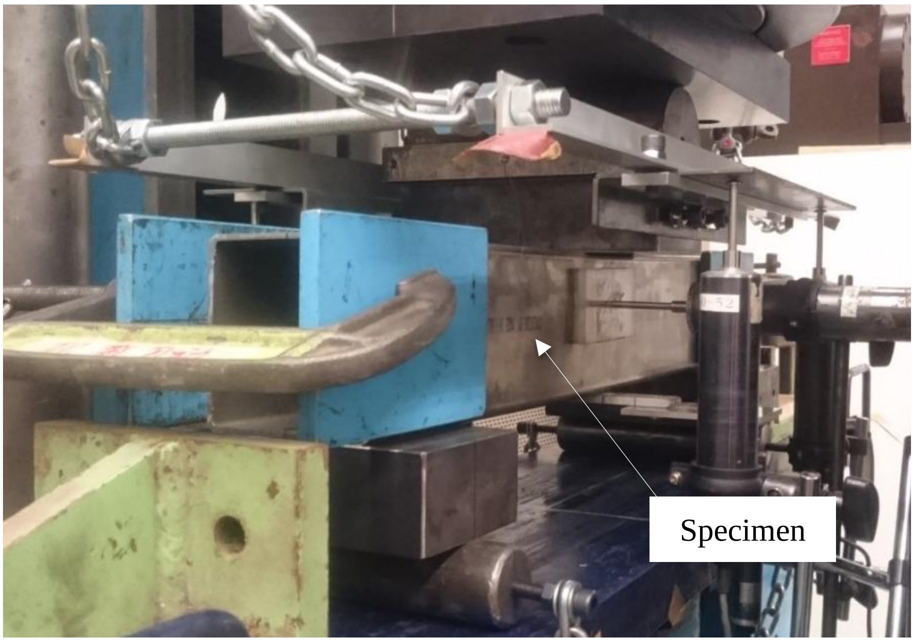

(a) Specimen in the test

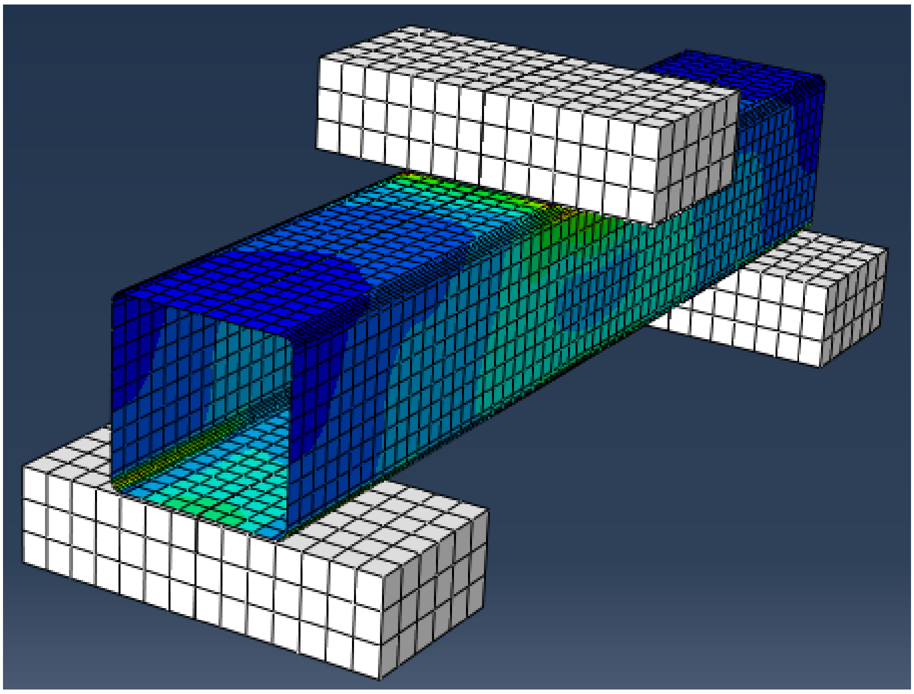

(b) 3-D view of specimen in FEM

Figure 4: Comparison of test and FEM for specimen IOF100×100×3.0N90

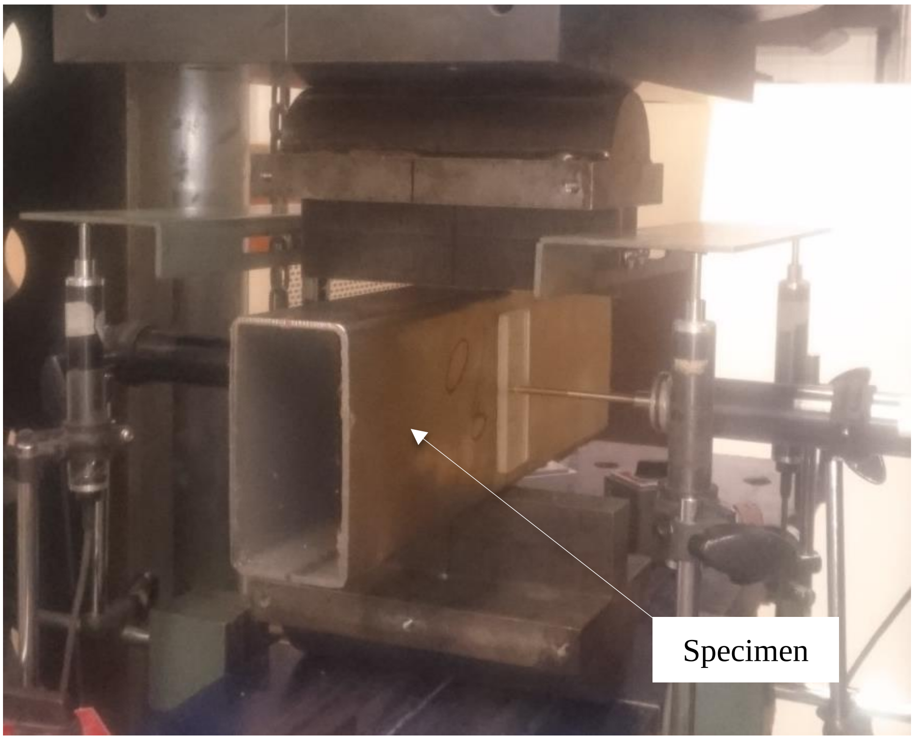

(a) Specimen in the test

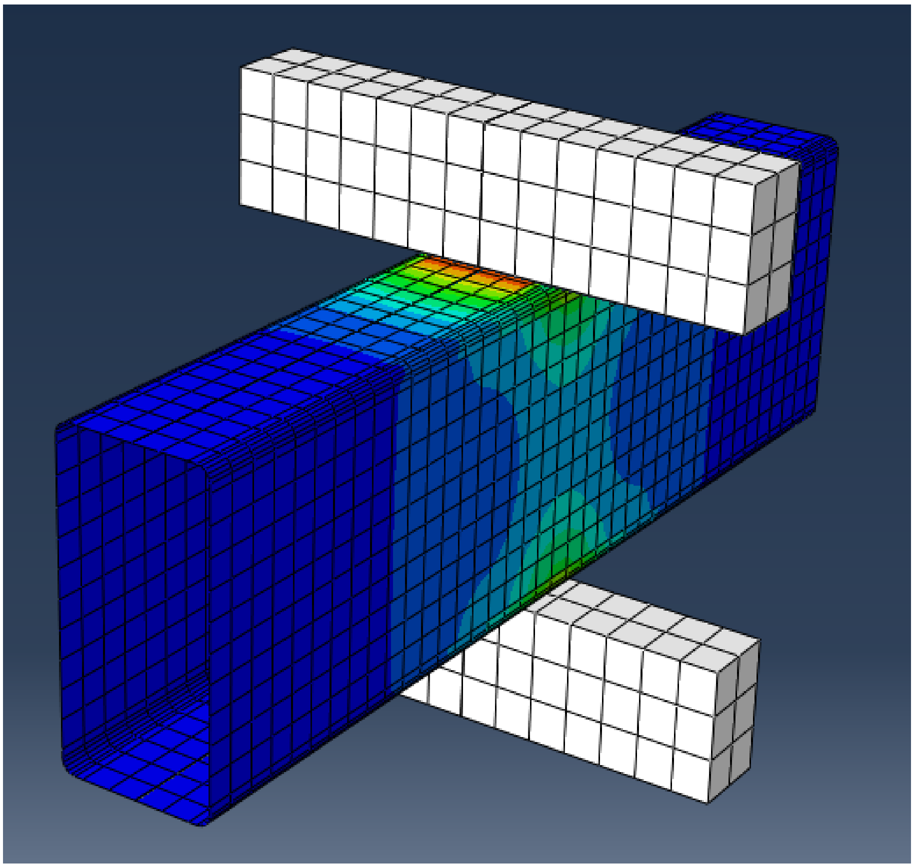

(b) 3-D view of specimen in FEM

Figure 5: Comparison of test and FEM for specimen ITF120×60×3.0N30

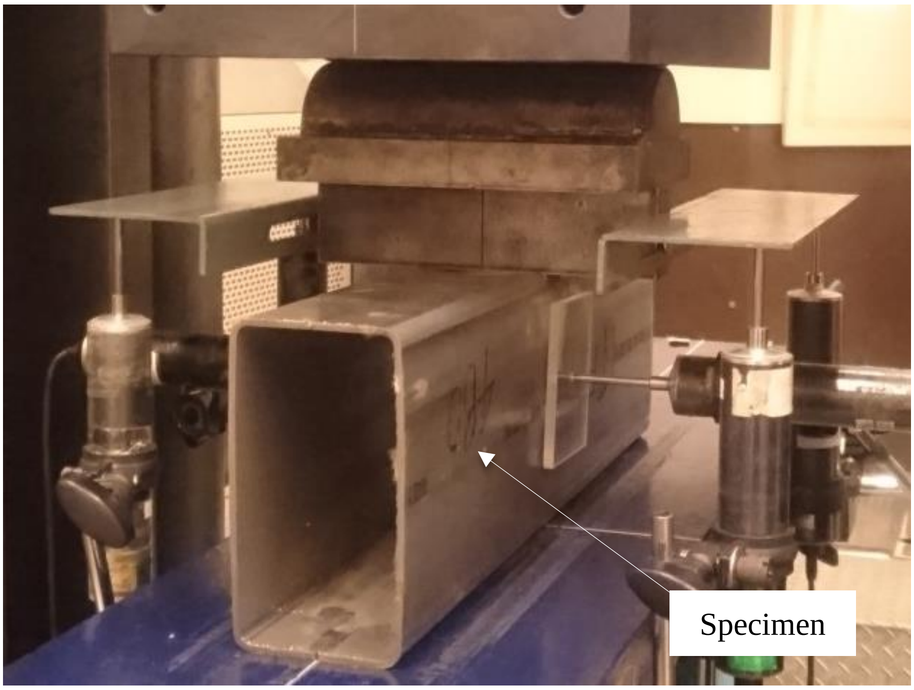

(a) Specimen in the test

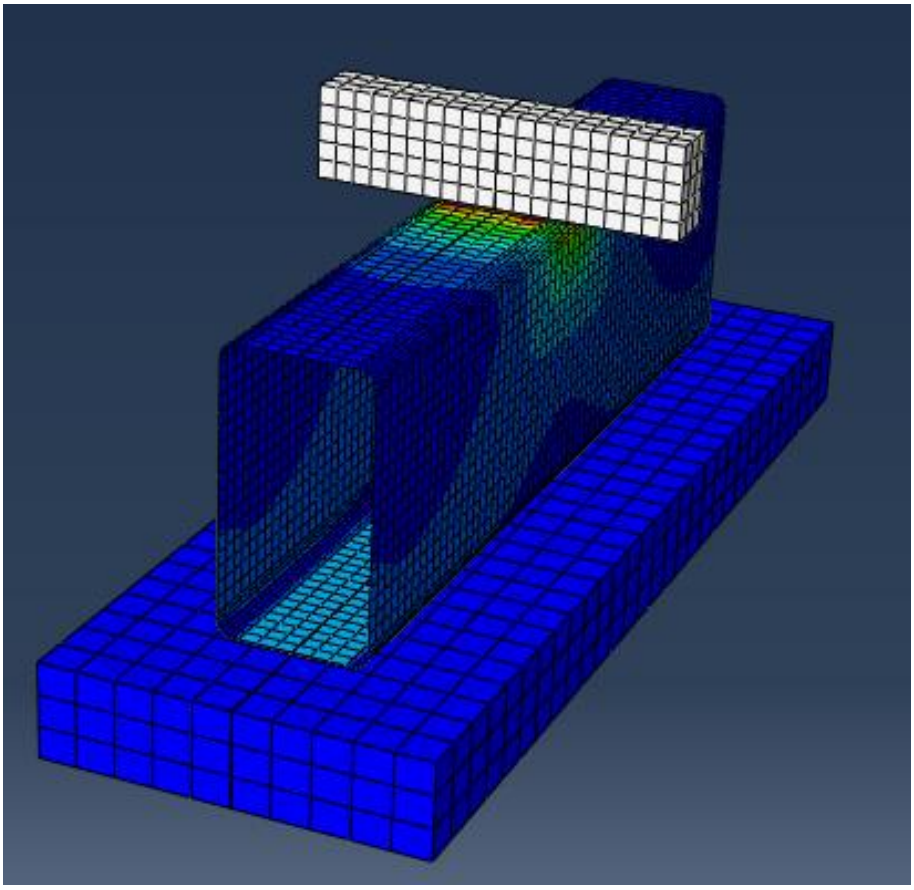

(b) 3-D view of specimen in FEM

Figure 6: Comparison of test and FEM for specimen IL150×80×3.0N30

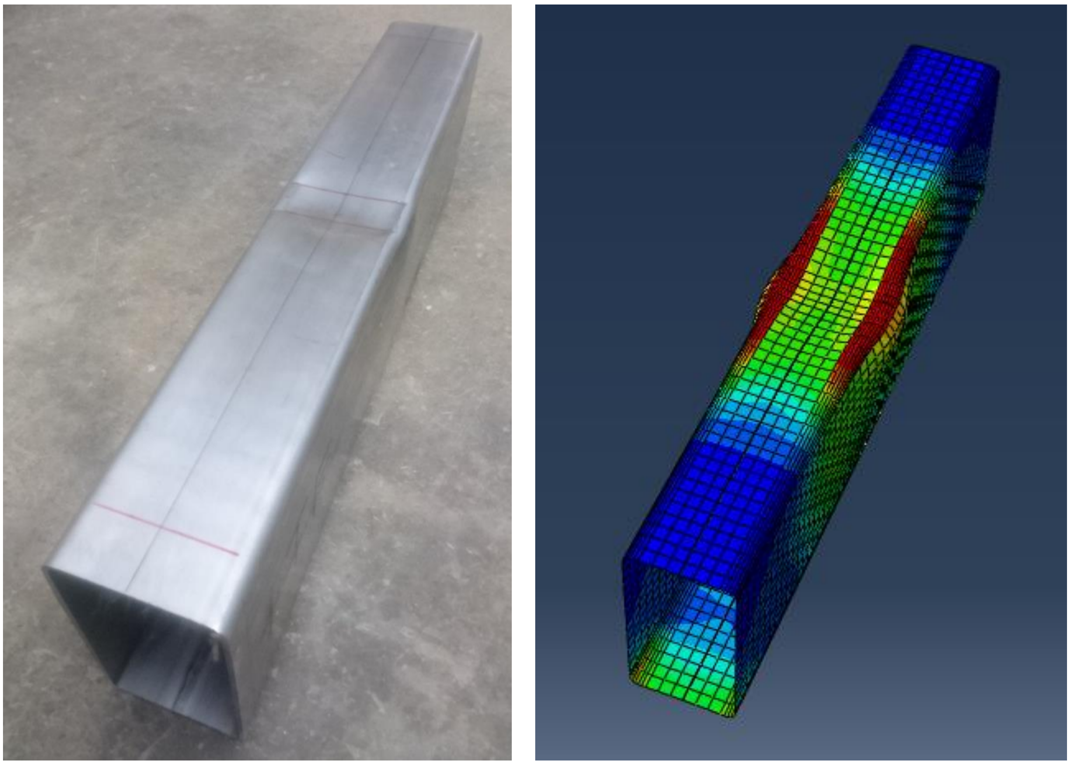

Figure 7: Failure mode of specimen IOF150×80×3.0N30 by test (*left*) and FEA (*right*)

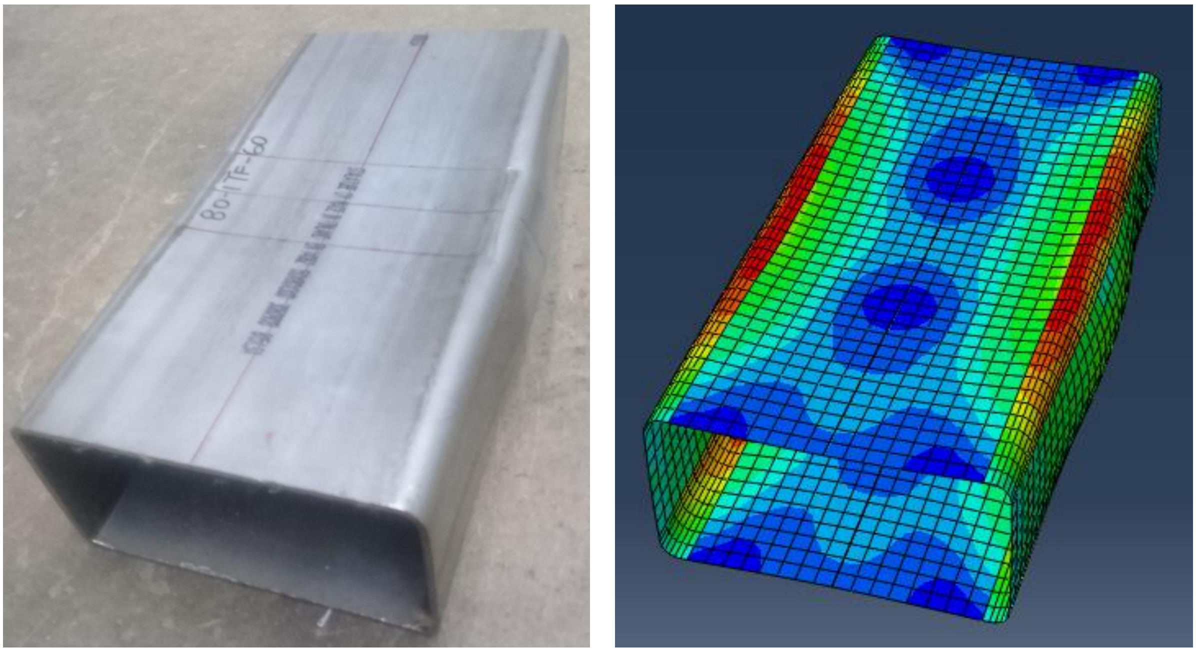

Figure 8: Failure mode of specimen ITF80×150×3.0N60 by test (*left*) and FEA (*right*)

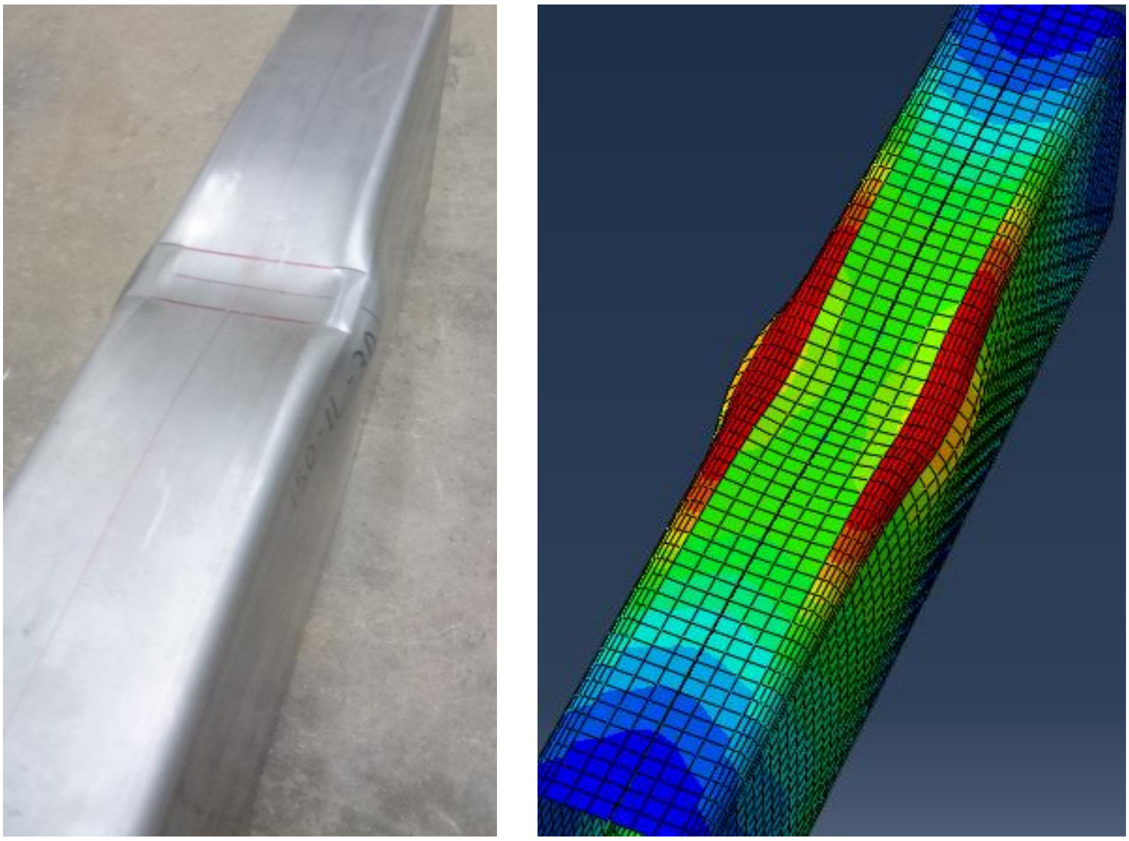

Figure 9: Failure mode of specimen IL150×80×3.0N30 by test (*left*) and FEA (*right*)

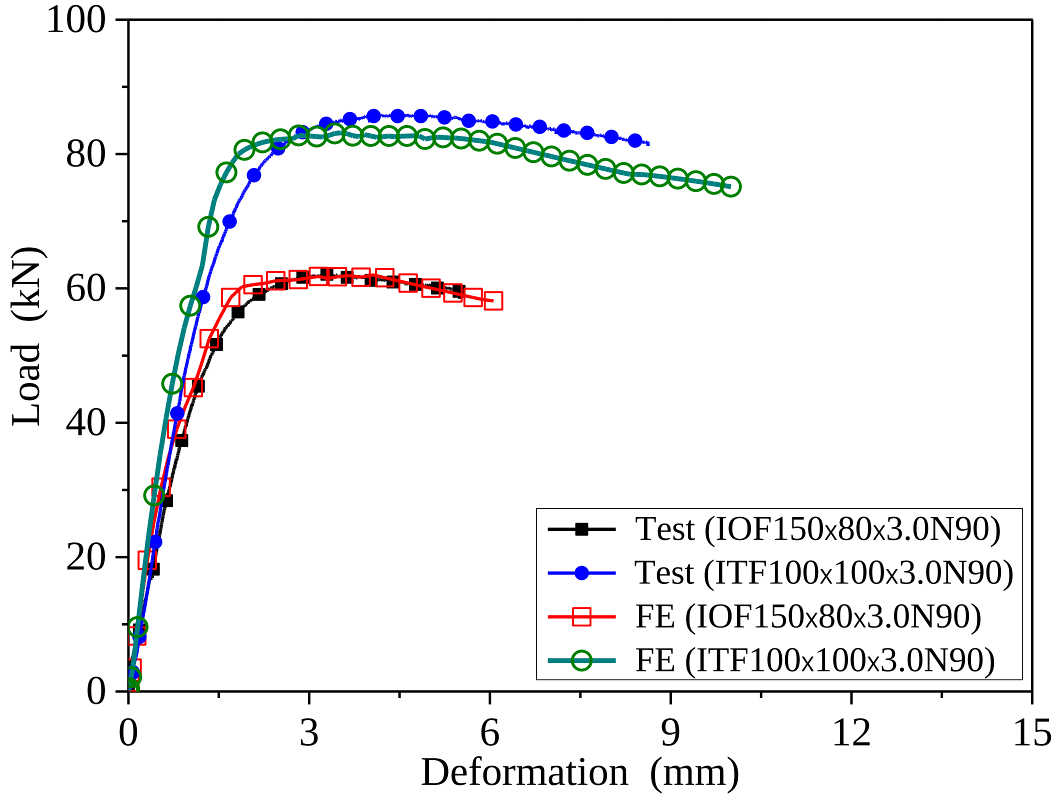

Figure 10: Comparison of load-deformation curves obtained from tests and finite element analysis

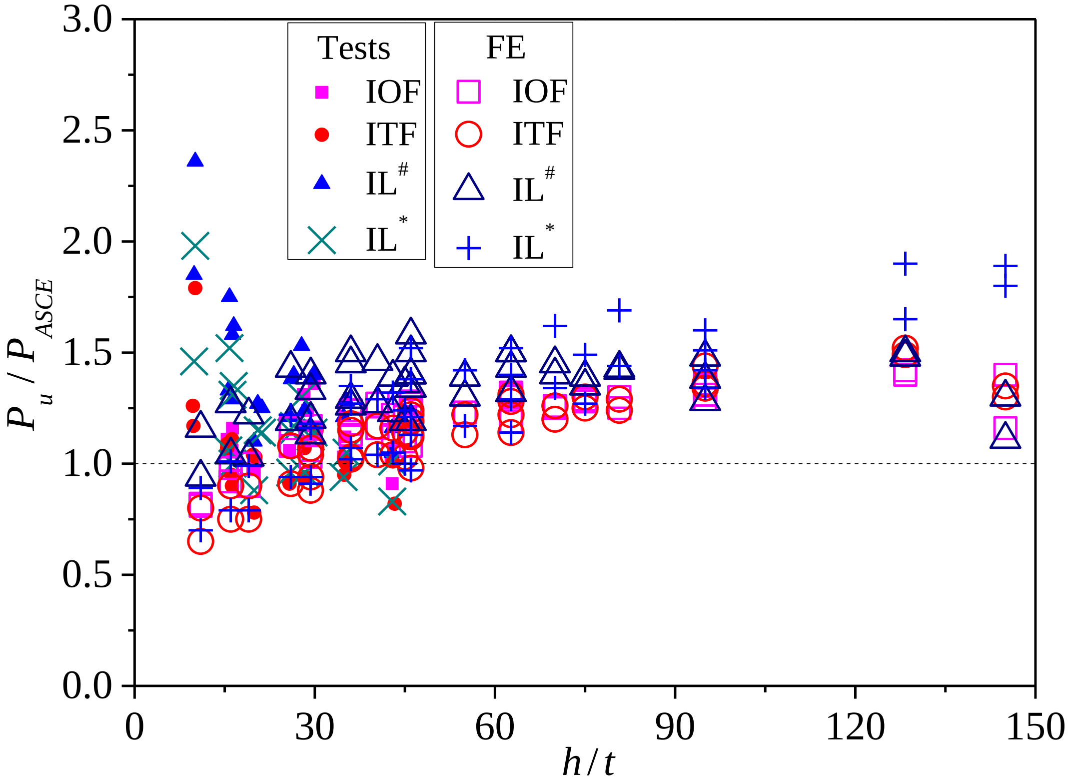

Figure 11: Comparison of test and FE results with ASCE predictions [19]

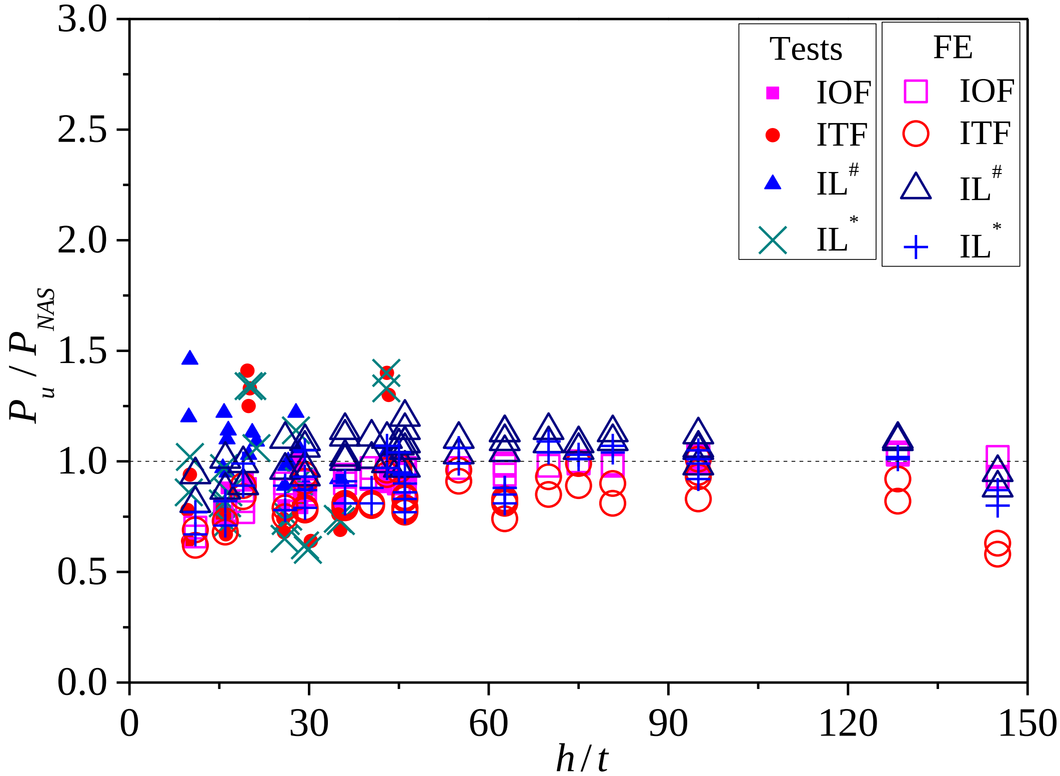

Figure 12: Comparison of test and FE results with NAS predictions [24]

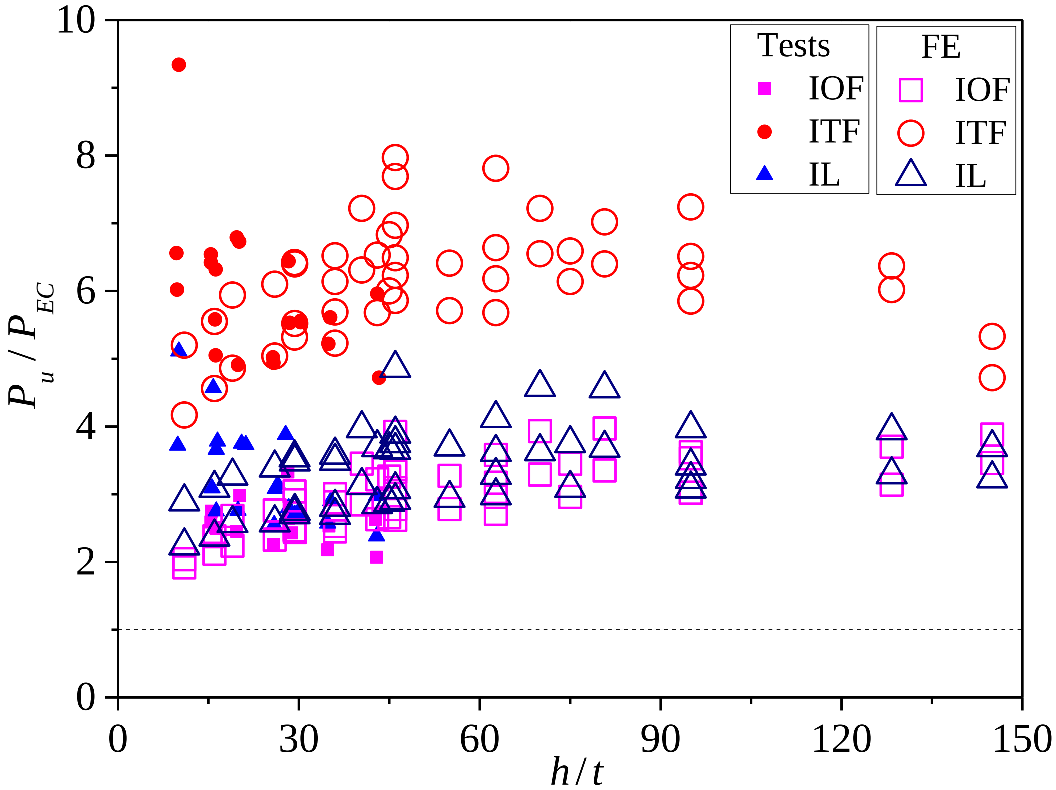

Figure 13: Comparison of test and FE results with EC3-1.3 predictions [39]

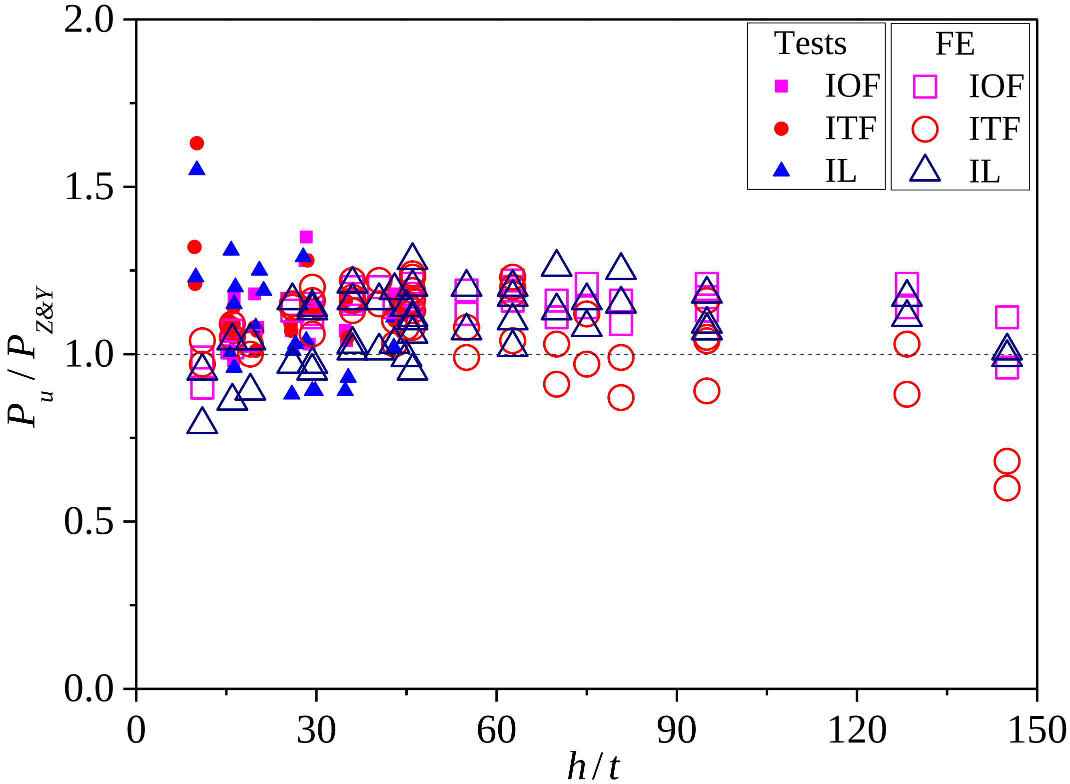

Figure 14: Comparison of test and FE results with predictions by Zhou and Young [25]

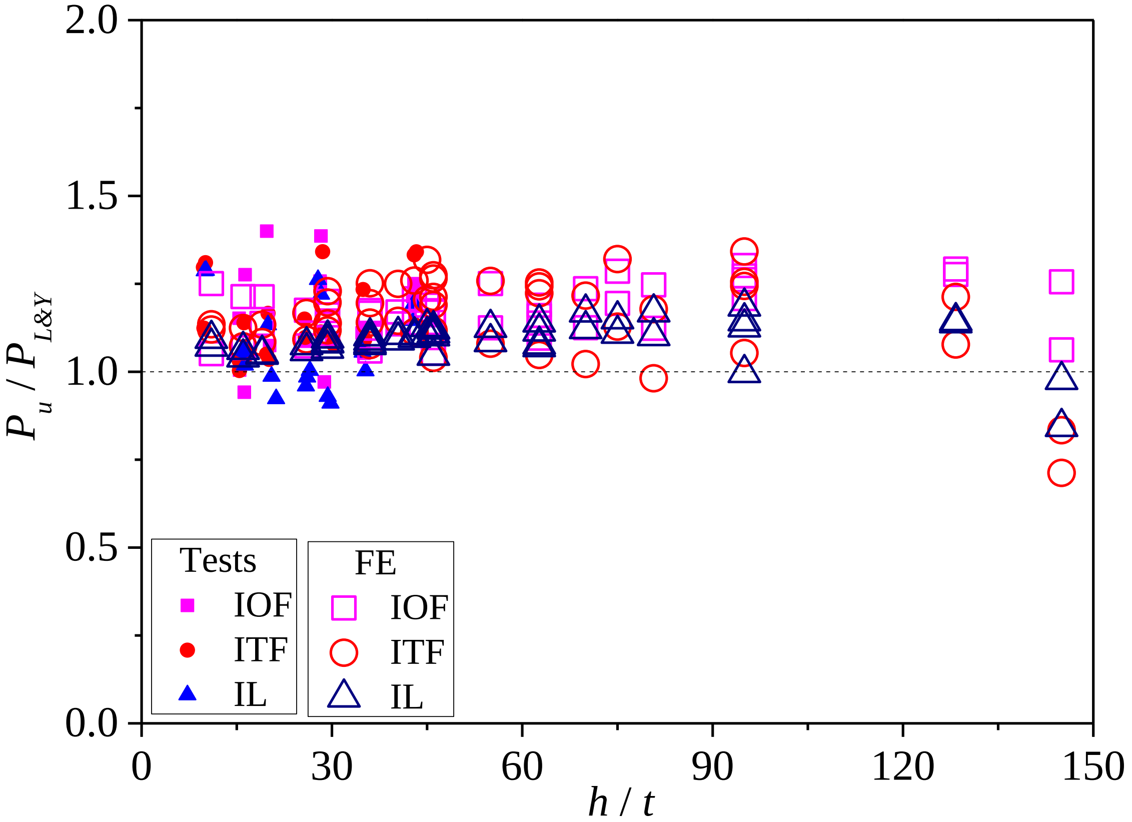

Figure 15: Comparison of test and FE results with predictions by Li and Young [31,32]

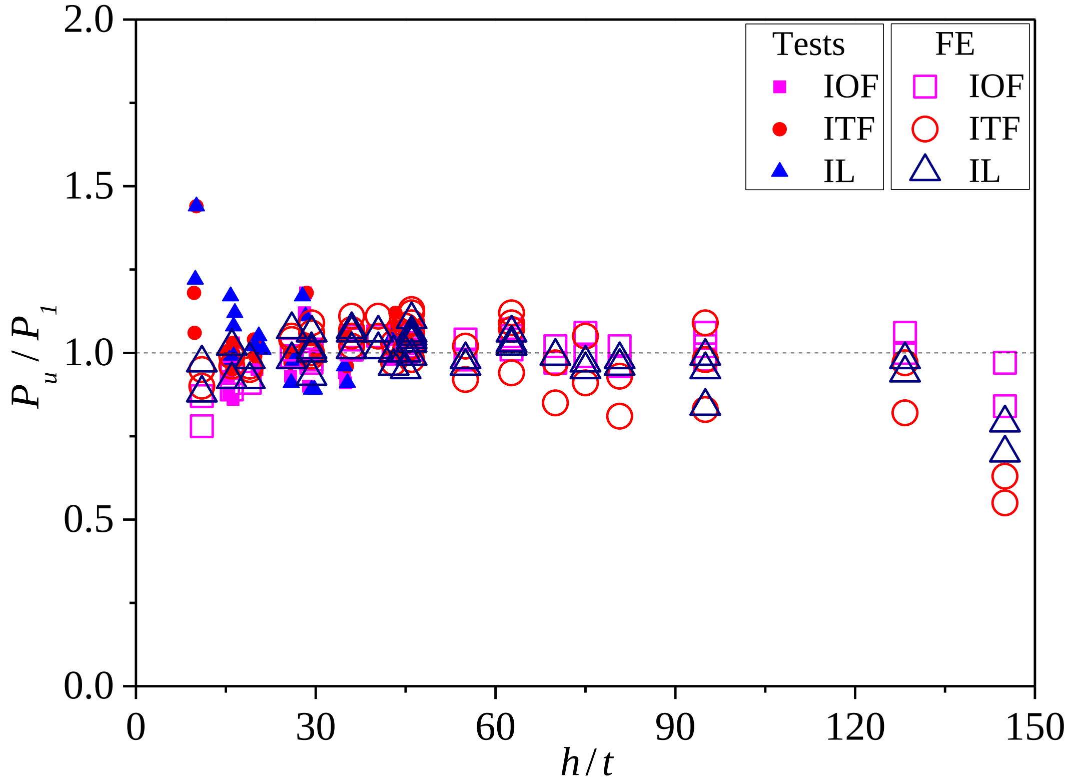

Figure 16: Comparison of test and FE results with predictions by unified design equation using newly proposed coefficients

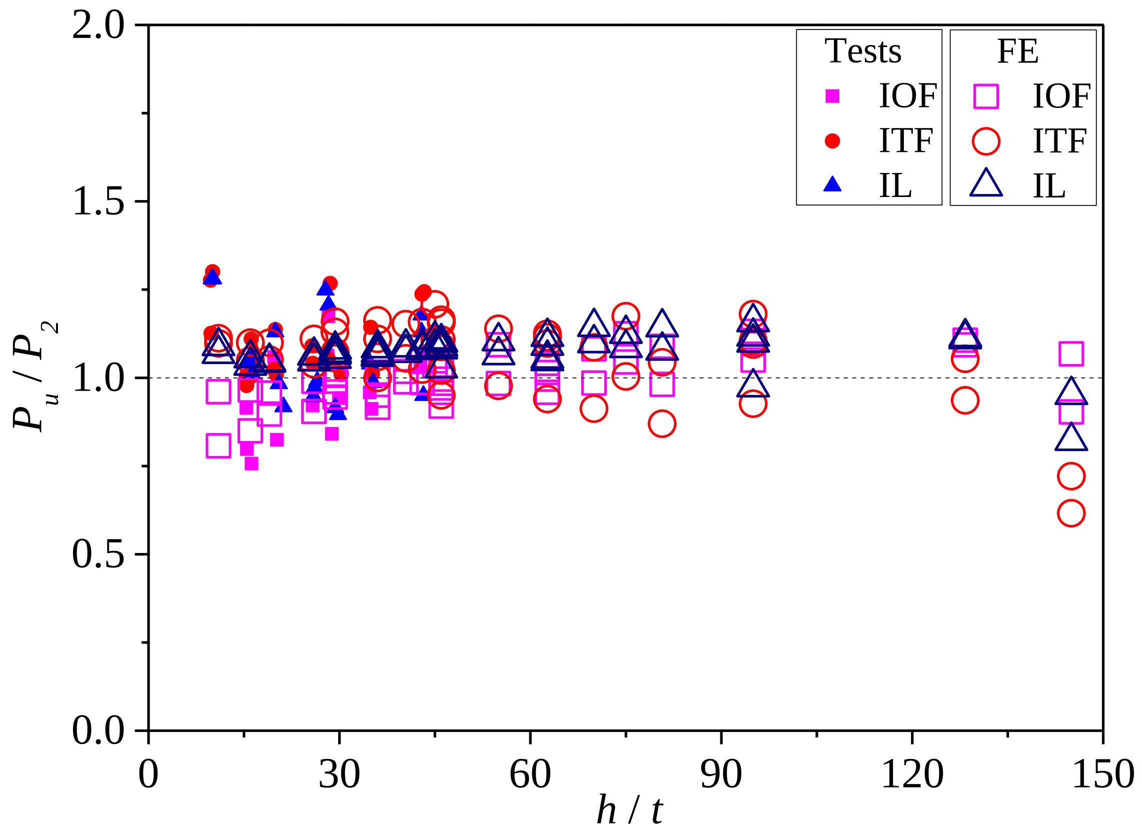

Figure 17: Comparison of test and FE results with predictions by DSM using newly proposed coefficients

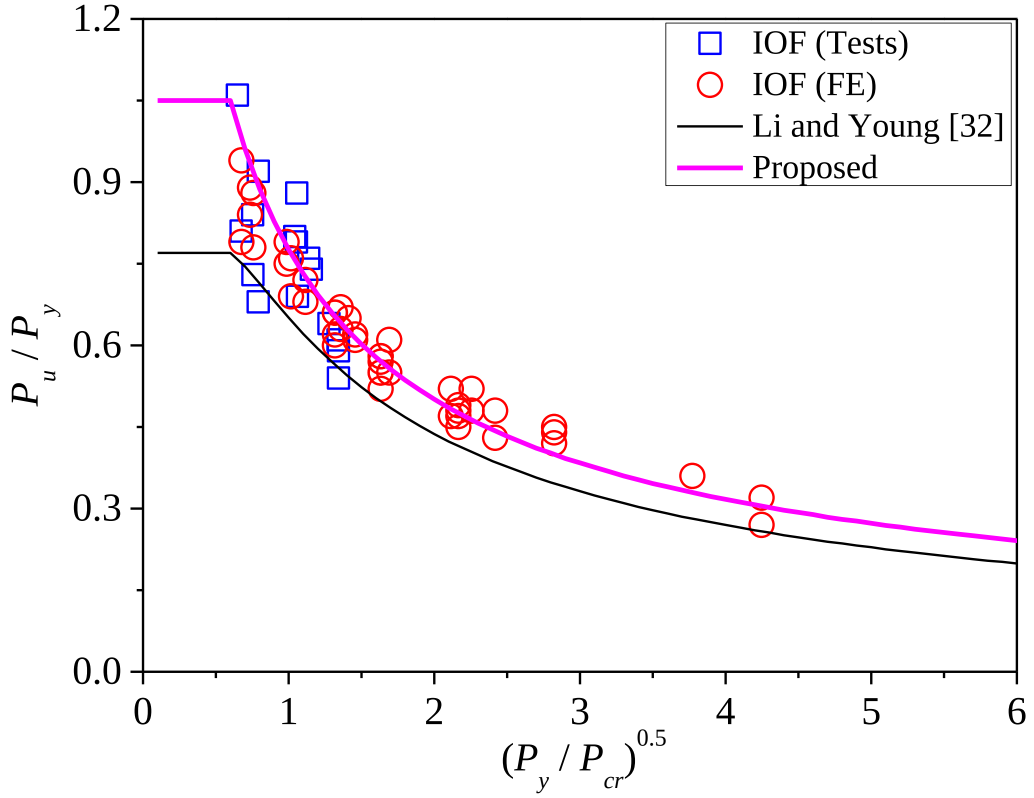

Figure 18: Comparison of test and numerical results with DSM curves for IOF loading condition

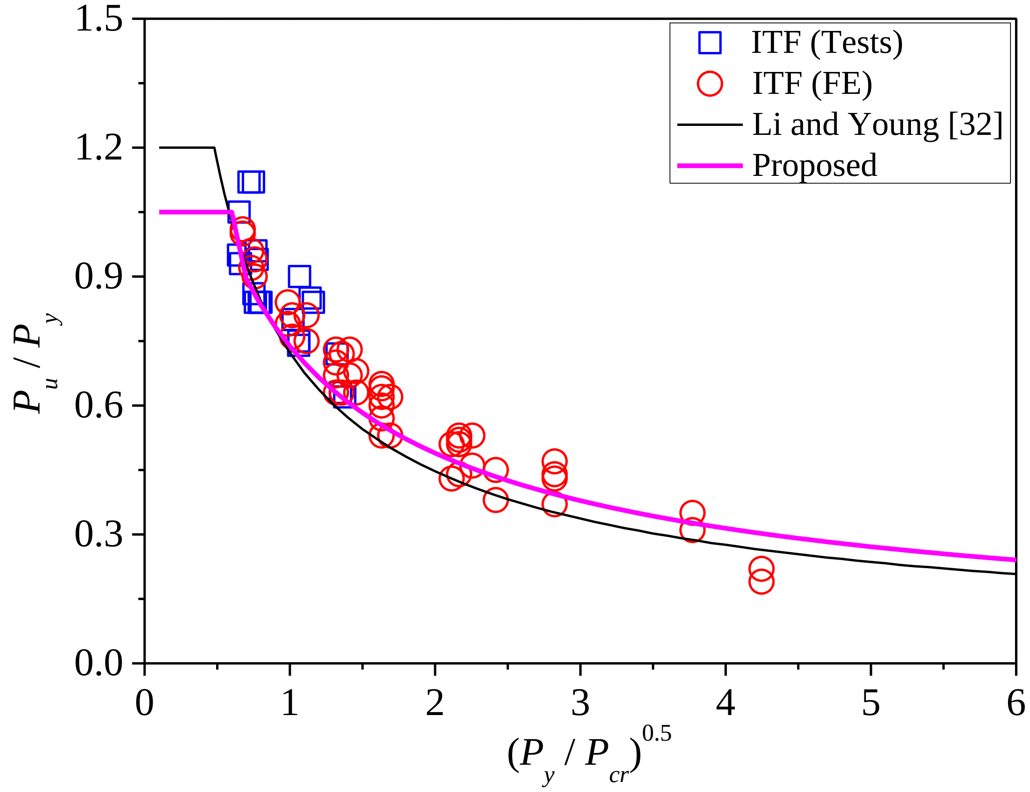

Figure 19: Comparison of test and numerical results with DSM curves for ITF loading condition

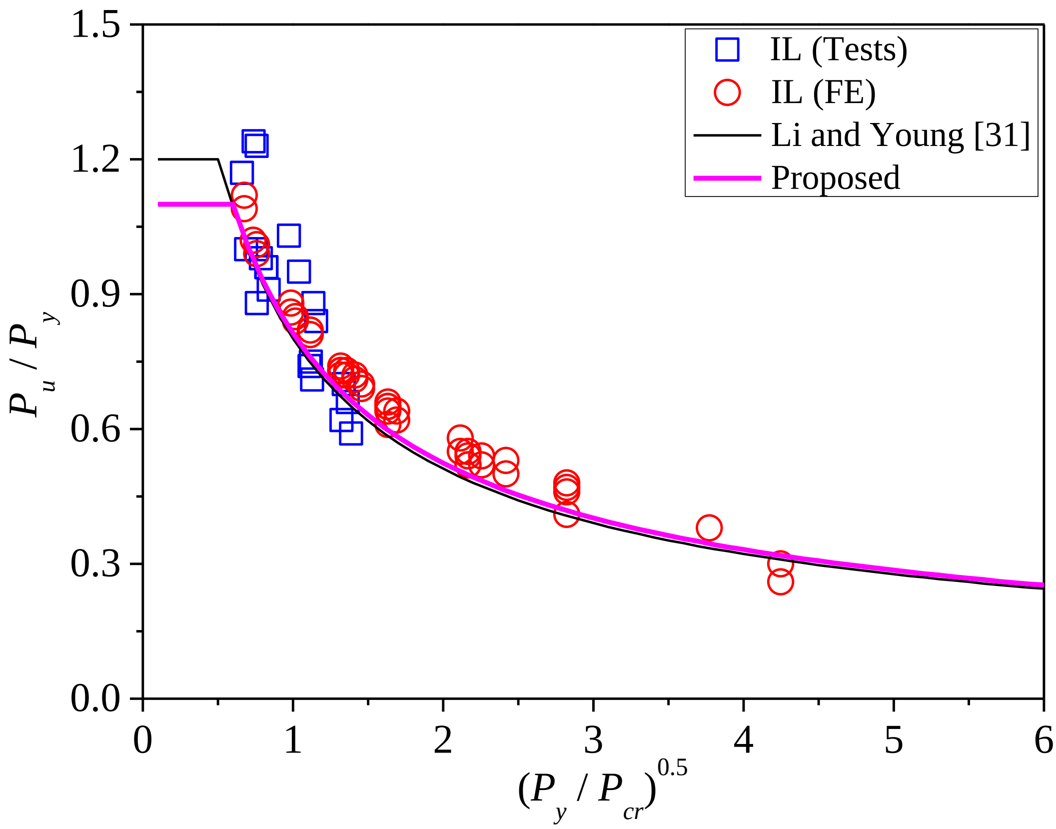

Figure 20: Comparison of test and numerical results with DSM curves for IL condition

Table 1: Material properties of cold-formed lean duplex stainless steel

(a) Material properties of flat coupons [23]

Stainless steel grade	Section $H \times B \times t$ (mm)	E_T GPa	E_C GPa	$f_{0.2,T}$ MPa	$f_{0.2,C}$ MPa	$\varepsilon_{f,T}$ %
EN 1.4162	50×20×1.5	194	212	656	611	42.2
EN 1.4062	60×40×2.0	199	211	600	627	40.3
	60×120×3.0	206	215	620	727	38.5
	80×150×3.0	194	214	491	546	43.3
	100×100×3.0	202	209	557	551	43.1
	120×60×3.0	206	215	620	611	38.5
	150×80×3.0	194	208	491	518	43.3

(b) Material properties of corner coupons

Stainless steel grade	Section $H \times B \times t$ (mm)	E_T GPa	$f_{0.2,T}$ MPa	$\varepsilon_{f,T}$ %
EN 1.4062	60×40×2.0[a]	199	797	12.1
	60×120×3.0[a]	207	793	14.7
	80×150×3.0[b]	196	754	20.0
	100×100×3.0[b]	195	784	17.0
	120×60×3.0[a]	207	793	14.7
	150×80×3.0[b]	196	754	20.0

Note: [a] means data from Ref. [35]; [b] means data from Ref. [36].

Table 2: Comparison of test strengths with FE strengths for IOF loading condition

Specimen	P_t (kN)	P_{FEA-1} (kN)	P_{FEA-2} (kN)	P_t/P_{FEA-1}	P_t/P_{FEA-2}
IOF60×40×2.0N30	29.3*	31.0	31.3	0.95	0.94
IOF60×120×3.0N60	73.5*	76.1	80.7	0.97	0.91
IOF60×120×3.0N90	77.5*	80.2	84.3	0.97	0.92
IOF80×150×3.0N60	57.7*	57.6	58.0	1.00	0.99
IOF80×150×3.0N150	70.6*	70.3	72.7	1.00	0.97
IOF100×100×3.0N30	70.7*	61.5	61.8	1.15	1.14
IOF100×100×3.0N90	89.1*	82.2	82.9	1.08	1.07
IOF100×100×3.0N90-r	89.5*	82.7	83.5	1.08	1.07
IOF120×60×3.0N30	61.1*	61.4	61.5	1.00	0.99
IOF120×60×3.0N60	71.6*	77.1	77.4	0.93	0.93
IOF150×80×3.0N30	48.4*	49.2	48.9	0.98	0.99
IOF150×80×3.0N90	62.1*	62.0	63.3	1.00	0.98
			Mean	1.01	0.99
			COV	0.064	0.072

Note: "*" means result presented in Ref. [23].

Table 3: Comparison of test strengths with FE strengths for ITF loading condition

Specimen	P_t (kN)	P_{FEA-1} (kN)	P_{FEA-2} (kN)	P_t/P_{FEA-1}	P_t/P_{FEA-2}
ITF60×40×2.0N30	31.7*	32.4	33	0.98	0.96
ITF60×40×2.0N30-r	31.7*	33.7	34.3	0.94	0.92
ITF60×120×3.0N60	77.8*	81.3	87.9	0.96	0.89
ITF60×120×3.0N90	92.0*	97.4	104.9	0.94	0.88
ITF60×120×3.0N90-r	91.0*	99	106.7	0.92	0.85
ITF80×150×3.0N60	57.3*	54.9	57.7	1.04	0.99
ITF80×150×3.0N150	78.5*	80.6	84.3	0.97	0.93
ITF80×150×3.0N150-r	78.9*	79.8	83.3	0.99	0.95
ITF100×100×3.0N30	72.4*	66.7	66.4	1.09	1.09
ITF100×100×3.0N90	85.9*	83.2	83.9	1.03	1.02
ITF120×60×3.0N30	73.4*	70.7	70.6	1.04	1.04
ITF120×60×3.0N60	78.9*	88.2	87.9	0.89	0.90
ITF150×80×3.0N30	54.8*	57.9	54.2	0.95	1.01
ITF150×80×3.0N90	69.6*	70.4	72.3	0.99	0.96
			Mean	0.98	0.96
			COV	0.054	0.072

Note: "*" means result presented in Ref. [23].

Table 4: Comparison of test strengths with FE strengths for IL condition

Specimen	P_t (kN)	P_{FEA-1} (kN)	P_{FEA-2} (kN)	P_t/P_{FEA-1}	P_t/P_{FEA-2}
IL60×40×2.0N30	34.0*	37.4	37.6	0.91	0.90
IL60×40×2.0N50	40.2*	44.0	44.4	0.91	0.91
IL60×40×2.0N50-r	39.8*	42.9	43.3	0.93	0.92
IL60×120×3.0N60	86.6*	88.1	94.9	0.98	0.91
IL60×120×3.0N120	128.8*	126.5	137.9	1.02	0.93
IL80×150×3.0N60	65.2*	64.9	65.7	1.00	0.99
IL80×150×3.0N150	89.3*	98.7	103.0	0.90	0.87
IL80×150×3.0N150-r	88.7*	90.0	94.7	0.99	0.94
IL100×100×3.0N30	74.3*	67.0	67.1	1.11	1.11
IL100×100×3.0N90	102.0*	90.7	91.8	1.12	1.11
IL120×60×3.0N30	73.4*	68.7	68.0	1.07	1.08
IL120×60×3.0N60	81.5*	86.7	87.0	0.94	0.94
IL150×80×3.0N30	55.7*	53.4	53.3	1.04	1.05
IL150×80×3.0N90	70.3*	70.3	71.3	1.00	0.99
			Mean	1.00	0.97
			COV	0.073	0.083

Note: "*" means result presented in Ref. [23].

Table 5: Summary of FE verifications

Loading conditions	Number		P_t/P_{FEA-1}	P_t/P_{FEA-2}
IOF, ITF, IL	40	Mean	0.99	0.97
		COV	0.064	0.076

Table 6: Design of CFLDSS specimens for parametric study

Section (H×B×t)	N (mm)	r_i/t	h/t	N/t	N/h
60×60×1.5	30	1.0	36.0	20.0	0.56
60×60×1.5	60	1.0	36.0	40.0	1.11
60×60×2.0	30	1.0	26.0	15.0	0.58
60×60×2.0	60	1.0	26.0	30.0	1.15
60×60×3.0	30	1.0	16.0	10.0	0.63
60×60×3.0	60	1.0	16.0	20.0	1.25
60×60×4.0	30	1.0	11.0	7.5	0.68
60×60×4.0	60	1.0	11.0	15.0	1.36
120×120×2.0	60	1.5	55.0	30.0	0.55
120×120×2.0	120	1.5	55.0	60.0	1.09
120×120×2.5	60	1.5	43.0	24.0	0.56
120×120×2.5	120	1.5	43.0	48.0	1.12
120×120×3.5	60	1.5	29.3	17.1	0.59
120×120×3.5	120	1.5	29.3	34.3	1.17
120×120×5.0	60	1.5	19.0	12.0	0.63
120×120×5.0	120	1.5	19.0	24.0	1.26
300×300×2.0	150	1.5	145.0	75.0	0.52
300×300×2.0	300	1.5	145.0	150.0	1.03
300×300×3.5	150	1.5	80.7	42.9	0.53
300×300×3.5	300	1.5	80.7	85.7	1.06
300×300×4.0	150	1.5	70.0	37.5	0.54
300×300×4.0	300	1.5	70.0	75.0	1.07
300×300×6.0	150	1.0	46.0	25.0	0.54
300×300×6.0	300	1.0	46.0	50.0	1.09
100×80×1.5	40	1.0	62.7	26.7	0.43
100×80×1.5	80	1.0	62.7	53.3	0.85
100×80×2.0	40	1.0	46.0	20.0	0.43
100×80×2.0	80	1.0	46.0	40.0	0.87
100×80×2.5	40	1.0	36.0	16.0	0.44
100×80×2.5	80	1.0	36.0	32.0	0.89
100×80×3.0	40	1.0	29.3	13.3	0.45
100×80×3.0	80	1.0	29.3	26.7	0.91
200×150×2.0	75	1.5	95.0	37.5	0.39
200×150×2.0	150	1.5	95.0	75.0	0.79
200×150×2.5	75	1.5	75.0	30.0	0.40
200×150×2.5	150	1.5	75.0	60.0	0.80
200×150×4.0	75	1.5	45.0	18.8	0.42
200×150×4.0	150	1.5	45.0	37.5	0.83
200×150×4.5	75	1.0	40.4	16.7	0.41
200×150×4.5	150	1.0	40.4	33.3	0.82
400×200×3.0	100	1.5	128.3	33.3	0.26
400×200×3.0	200	1.5	128.3	66.7	0.52
400×200×4.0	100	1.5	95.0	25.0	0.26
400×200×4.0	200	1.5	95.0	50.0	0.53
400×200×6.0	100	1.0	62.7	16.7	0.27
400×200×6.0	200	1.0	62.7	33.3	0.53
400×200×8.0	100	1.0	46.0	12.5	0.27
400×200×8.0	200	1.0	46.0	25.0	0.54

Table 7: Comparison of test and FE strengths with predicted strengths for IOF loading condition

Specimens	P_u (P_t or P_{FEA}) (kN)	P_u/P_{ASCE}	P_u/P_{EC}	P_u/P_{NAS}	$P_u/P_{Z\&Y}$	$P_u/P_{L\&Y}$	P_u/P_1	P_u/P_2
IOF40×60×2.0N30	31.4	1.16	2.49	0.88	1.17	1.28	1.03	1.03
IOF40×60×2.0N60	32.2	1.06	2.51	0.77	0.98	0.94	0.86	0.76
IOF50×20×1.5N30	21.1	1.36	2.65	0.87	1.14	1.09	0.99	0.94
IOF50×20×1.5N30-r	20.9	1.24	2.43	0.79	1.03	0.97	0.90	0.84
IOF60×40×2.0N30	29.3	1.06	2.26	0.80	1.07	1.09	0.93	0.92
IOF60×120×3.0N60	73.5	1.11	2.59	0.81	1.06	1.15	0.93	0.92
IOF60×120×3.0N90	77.5	1.11	2.75	0.79	1.01	1.00	0.88	0.80
IOF80×150×3.0N60	57.7	0.98	2.45	0.92	1.18	1.40	1.03	1.06
IOF80×150×3.0N150	70.6	1.01	2.98	0.90	1.08	1.07	0.95	0.83
IOF100×100×3.0N30	70.7	1.17	2.64	0.99	1.35	1.39	1.18	1.18
IOF100×100×3.0N90	89.1	1.31	3.33	1.02	1.28	1.26	1.12	1.06
IOF100×100×3.0N90-r	89.5	1.31	3.33	1.02	1.28	1.24	1.12	1.06
IOF120×60×3.0N30	61.1	1.03	2.18	0.79	1.07	1.11	0.94	0.96
IOF120×60×3.0N60	71.6	1.12	2.53	0.81	1.04	1.05	0.91	0.91
IOF150×80×3.0N30	48.4	0.91	2.07	0.89	1.18	1.25	1.04	1.07
IOF150×80×3.0N90	62.1	1.02	2.63	0.92	1.12	1.21	0.98	1.04
IOF60×60×1.5N30	17.8	1.18	2.45	0.93	1.20	1.17	1.05	1.02
IOF60×60×1.5N60	21.0	1.24	2.88	0.94	1.15	1.06	1.01	0.92
IOF60×60×2.0N30	28.4	1.08	2.33	0.87	1.15	1.17	1.01	0.99
IOF60×60×2.0N60	33.6	1.16	2.76	0.90	1.13	1.07	0.99	0.91
IOF60×60×3.0N30	53.9	0.92	2.12	0.78	1.07	1.21	0.94	0.97
IOF60×60×3.0N60	60.6	0.98	2.38	0.77	1.02	1.07	0.89	0.85
IOF60×60×4.0N30	83.1	0.81	1.92	0.70	0.99	1.25	0.87	0.96
IOF60×60×4.0N60	88.3	0.82	2.04	0.66	0.90	1.05	0.78	0.81
IOF120×120×2.0N60	33.1	1.23	2.78	0.97	1.19	1.25	1.04	1.09
IOF120×120×2.0N120	38.9	1.23	3.27	0.97	1.12	1.12	0.98	0.98
IOF120×120×2.5N60	46.8	1.13	2.63	0.91	1.14	1.21	1.00	1.05
IOF120×120×2.5N120	57.4	1.22	3.22	0.96	1.14	1.14	1.00	0.99
IOF120×120×3.5N60	81.2	1.03	2.47	0.85	1.11	1.20	0.97	1.01
IOF120×120×3.5N120	100.0	1.14	3.04	0.91	1.12	1.14	0.98	0.96
IOF120×120×5.0N60	142.9	0.90	2.24	0.77	1.04	1.21	0.91	0.96
IOF120×120×5.0N120	171.0	1.00	2.68	0.82	1.04	1.14	0.91	0.90
IOF300×300×2.0N150	41.2	1.40	3.46	1.02	1.11	1.26	0.97	1.07
IOF300×300×2.0N300	46.0	1.16	3.88	0.93	0.96	1.06	0.84	0.90
IOF300×300×3.5N150	110.4	1.30	3.35	0.99	1.16	1.25	1.02	1.09
IOF300×300×3.5N300	130.9	1.25	3.97	0.98	1.09	1.12	0.96	0.98

IOF300×300×4.0N150	138.5	1.26	3.29	0.98	1.16	1.24	1.02	1.08
IOF300×300×4.0N300	165.4	1.25	3.93	0.98	1.11	1.13	0.97	0.99
IOF300×300×6.0N150	305.4	1.24	3.33	0.96	1.21	1.17	1.05	1.02
IOF300×300×6.0N300	359.6	1.28	3.92	0.97	1.15	1.05	1.01	0.92
IOF100×80×1.5N40	19.7	1.30	2.71	0.99	1.22	1.19	1.07	1.04
IOF100×80×1.5N80	23.0	1.32	3.17	0.99	1.16	1.10	1.01	0.96
IOF100×80×2.0N40	31.9	1.21	2.62	0.94	1.21	1.17	1.06	1.03
IOF100×80×2.0N80	37.7	1.27	3.09	0.96	1.17	1.10	1.02	0.96
IOF100×80×2.5N40	46.2	1.13	2.53	0.90	1.18	1.17	1.04	1.01
IOF100×80×2.5N80	54.8	1.22	3.00	0.93	1.16	1.10	1.01	0.95
IOF100×80×3.0N40	62.1	1.06	2.44	0.87	1.15	1.16	1.01	0.99
IOF100×80×3.0N80	74.2	1.17	2.91	0.91	1.15	1.11	1.01	0.95
IOF200×150×2.0N75	35.9	1.36	3.02	1.03	1.21	1.30	1.06	1.13
IOF200×150×2.0N150	42.0	1.31	3.53	1.01	1.13	1.21	0.98	1.05
IOF200×150×2.5N75	52.7	1.29	2.96	1.00	1.21	1.29	1.06	1.13
IOF200×150×2.5N150	61.4	1.28	3.45	0.99	1.14	1.19	0.99	1.05
IOF200×150×4.0N75	111.9	1.10	2.66	0.90	1.14	1.21	1.00	1.05
IOF200×150×4.0N150	137.5	1.21	3.26	0.95	1.15	1.19	1.01	1.03
IOF200×150×4.5N75	153.0	1.16	2.85	0.92	1.20	1.17	1.05	1.02
IOF200×150×4.5N150	185.4	1.27	3.45	0.97	1.20	1.14	1.05	0.99
IOF400×200×3.0N100	78.0	1.42	3.14	1.04	1.21	1.29	1.06	1.11
IOF400×200×3.0N200	91.8	1.40	3.70	1.03	1.14	1.28	1.00	1.09
IOF400×200×4.0N100	127.3	1.29	3.02	1.00	1.21	1.26	1.06	1.10
IOF400×200×4.0N200	152.6	1.35	3.62	1.02	1.17	1.27	1.02	1.11
IOF400×200×6.0N100	271.7	1.19	2.96	0.94	1.20	1.14	1.05	1.00
IOF400×200×6.0N200	328.4	1.31	3.58	0.98	1.19	1.16	1.04	1.02
IOF400×200×8.0N100	436.3	1.08	2.78	0.88	1.16	1.11	1.02	0.97
IOF400×200×8.0N200	529.2	1.21	3.37	0.94	1.18	1.14	1.03	1.00
Mean		1.17	2.91	0.92	1.14	1.17	0.99	0.99
COV		0.120	0.174	0.095	0.070	0.077	0.070	0.086
Resistance factor, ϕ		0.70	0.91	0.90	0.70	0.85	0.85	0.85
Reliability index, β		3.85	5.51	2.07	4.02	3.31	2.70	2.63

Table 8: Comparison of test and FE strengths with predicted strengths for ITF loading condition

Specimens	P_u (P_t or P_{FEA}) (kN)	P_u/P_{ASCE}	P_u/P_{EC}	P_u/P_{NAS}	$P_u/P_{Z\&Y}$	$P_u/P_{L\&Y}$	P_u/P_1	P_u/P_2
ITF20×50×1.5N30	25.6	1.17	6.02	0.64	1.21	1.12	1.06	1.13
ITF20×50×1.5N30-r	26.1	1.26	6.56	0.78	1.32	1.30	1.18	1.28
ITF20×50×1.5N50	36.5	1.79	9.34	0.94	1.63	1.31	1.44	1.30
ITF40×60×2.0N30	31.4	0.90	5.05	0.72	1.09	1.14	1.00	1.11
ITF40×60×2.0N60	39.8	1.11	6.32	0.76	1.14	1.03	1.03	1.00
ITF50×20×1.5N30	21.5	1.16	5.56	0.64	1.12	1.08	1.00	1.01
ITF50×20×1.5N30-r	21.4	1.15	5.54	0.64	1.12	1.08	0.99	1.01
ITF60×40×2.0N30	31.7	0.92	5.02	0.74	1.09	1.15	1.00	1.09
ITF60×40×2.0N30-r	31.7	0.91	4.94	0.68	1.07	1.10	0.97	1.04
ITF60×120×3.0N60	77.8	0.95	5.58	0.67	1.05	1.03	0.95	1.00
ITF60×120×3.0N90	92.0	1.09	6.54	0.78	1.10	1.03	1.00	1.01
ITF60×120×3.0N90-r	91.0	1.07	6.42	0.75	1.08	1.00	0.98	0.98
ITF80×150×3.0N60	57.3	0.78	4.91	1.25	1.01	1.17	0.99	1.14
ITF80×150×3.0N150	78.5	1.03	6.73	1.33	1.07	1.03	1.03	1.01
ITF80×150×3.0N150-r	78.9	1.04	6.79	1.41	1.08	1.05	1.04	1.02
ITF100×100×3.0N30	72.4	0.94	5.53	0.86	1.28	1.34	1.18	1.27
ITF100×100×3.0N90	85.9	1.07	6.44	0.81	1.14	1.11	1.04	1.05
ITF120×60×3.0N30	73.4	0.95	5.22	0.76	1.16	1.23	1.06	1.14
ITF120×60×3.0N60	78.9	1.01	5.61	0.69	1.05	1.09	0.96	1.01
ITF150×80×3.0N30	54.8	0.82	4.72	1.30	1.15	1.34	1.12	1.24
ITF150×80×3.0N90	69.6	1.01	5.96	1.40	1.10	1.33	1.08	1.24
ITF60×60×1.5N30	18.9	1.03	5.23	0.79	1.17	1.19	1.07	1.11
ITF60×60×1.5N60	22.1	1.18	6.14	0.79	1.13	1.08	1.02	1.00
ITF60×60×2.0N30	30.4	0.91	5.04	0.75	1.14	1.17	1.04	1.11
ITF60×60×2.0N60	36.8	1.08	6.10	0.79	1.15	1.09	1.05	1.04
ITF60×60×3.0N30	57.5	0.75	4.56	0.68	1.05	1.12	0.96	1.10
ITF60×60×3.0N60	70.1	0.90	5.55	0.73	1.09	1.07	0.99	1.05
ITF60×60×4.0N30	89.4	0.65	4.17	0.62	0.97	1.14	0.90	1.11
ITF60×60×4.0N60	111.4	0.80	5.20	0.69	1.04	1.12	0.95	1.10
ITF120×120×2.0N60	33.6	1.13	5.71	0.96	1.08	1.26	1.02	1.14
ITF120×120×2.0N120	37.7	1.22	6.41	0.91	0.99	1.08	0.92	0.98
ITF120×120×2.5N60	50.1	1.04	5.68	0.96	1.10	1.26	1.03	1.16
ITF120×120×2.5N120	57.7	1.16	6.53	0.94	1.03	1.11	0.97	1.02
ITF120×120×3.5N60	86.9	0.88	5.32	0.91	1.06	1.20	1.00	1.13
ITF120×120×3.5N120	104.8	1.04	6.42	0.94	1.06	1.12	0.99	1.06

ITF120×120×5.0N60	153.6	0.75	4.86	0.84	1.00	1.13	0.95	1.10
ITF120×120×5.0N120	187.4	0.90	5.94	0.89	1.03	1.08	0.96	1.05
ITF300×300×2.0N150	27.8	1.30	4.72	0.63	0.68	0.83	0.63	0.72
ITF300×300×2.0N300	31.4	1.35	5.33	0.58	0.60	0.71	0.55	0.62
ITF300×300×3.5N150	104.6	1.24	6.40	0.90	0.99	1.18	0.93	1.04
ITF300×300×3.5N300	114.6	1.29	7.02	0.81	0.87	0.98	0.81	0.87
ITF300×300×4.0N150	136.7	1.20	6.55	0.93	1.03	1.22	0.97	1.09
ITF300×300×4.0N300	150.8	1.26	7.22	0.85	0.91	1.02	0.85	0.91
ITF300×300×6.0N150	317.0	1.12	6.97	0.79	1.16	1.19	1.06	1.09
ITF300×300×6.0N300	362.5	1.24	7.97	0.77	1.08	1.04	0.98	0.95
ITF100×80×1.5N40	20.5	1.22	5.68	0.81	1.18	1.22	1.07	1.10
ITF100×80×1.5N80	22.2	1.28	6.18	0.74	1.04	1.05	0.94	0.94
ITF100×80×2.0N40	35.4	1.13	5.86	0.83	1.24	1.27	1.13	1.16
ITF100×80×2.0N80	39.2	1.22	6.49	0.79	1.13	1.12	1.02	1.02
ITF100×80×2.5N40	51.5	1.02	5.69	0.81	1.22	1.25	1.11	1.16
ITF100×80×2.5N80	59.0	1.15	6.52	0.80	1.16	1.14	1.05	1.06
ITF100×80×3.0N40	69.7	0.94	5.52	0.78	1.20	1.23	1.09	1.16
ITF100×80×3.0N80	80.9	1.07	6.40	0.79	1.16	1.14	1.06	1.07
ITF200×150×2.0N75	34.5	1.34	5.85	0.93	1.04	1.24	0.98	1.09
ITF200×150×2.0N150	36.7	1.36	6.23	0.83	0.89	1.05	0.83	0.93
ITF200×150×2.5N75	54.2	1.25	6.14	0.99	1.12	1.32	1.05	1.17
ITF200×150×2.5N150	58.2	1.30	6.59	0.89	0.97	1.13	0.91	1.00
ITF200×150×4.0N75	125.2	1.03	6.00	0.98	1.15	1.32	1.08	1.21
ITF200×150×4.0N150	142.7	1.14	6.83	0.96	1.08	1.21	1.01	1.11
ITF200×150×4.5N75	168.1	1.04	6.31	0.81	1.22	1.25	1.11	1.15
ITF200×150×4.5N150	192.3	1.17	7.22	0.80	1.15	1.14	1.05	1.06
ITF400×200×3.0N100	74.1	1.49	6.02	0.92	1.03	1.21	0.97	1.05
ITF400×200×3.0N200	78.4	1.52	6.37	0.82	0.88	1.08	0.82	0.94
ITF400×200×4.0N100	135.9	1.34	6.51	1.01	1.16	1.34	1.09	1.18
ITF400×200×4.0N200	151.1	1.44	7.24	0.95	1.05	1.26	0.98	1.10
ITF400×200×6.0N100	302.0	1.14	6.64	0.82	1.23	1.25	1.12	1.12
ITF400×200×6.0N200	355.2	1.31	7.81	0.83	1.20	1.24	1.09	1.11
ITF400×200×8.0N100	485.8	0.98	6.23	0.78	1.19	1.21	1.09	1.11
ITF400×200×8.0N200	599.2	1.19	7.69	0.84	1.23	1.26	1.12	1.16
Mean		1.11	6.09	0.85	1.09	1.15	1.01	1.07
COV		0.181	0.145	0.201	0.125	0.101	0.117	0.105
Resistance factor, ϕ		0.70	0.91	0.80	0.70	0.85	0.85	0.85
Reliability index, β		3.24	8.47	1.82	3.56	3.15	2.57	2.85

Table 9: Comparison of test and FE strengths with predicted strengths for IL condition

Specimens	P_u (P_t or P_{FEA})	P_u/P_{ASCE}		P_u/P_{EC}	P_u/P_{NAS}		$P_u/P_{Z\&Y}$	P_u/P_{DSM}	P_u/P_1	P_u/P_2
	(kN)	IOF#	ITF*		IOF#	ITF*				
IL20×50×1.5N30	29.9	1.85	1.46	3.72	1.20	0.86	1.23	1.29	1.22	1.28
IL20×50×1.5N50	41.1	2.36	1.98	5.11	1.46	1.02	1.55	1.29	1.44	1.28
IL40×60×2.0N30	35.9	1.29	1.00	2.75	0.95	0.72	0.96	1.06	0.99	1.06
IL40×60×2.0N60	48.4	1.62	1.35	3.78	1.14	0.86	1.20	1.07	1.12	1.06
IL40×60×2.0N60-r	48.4	1.58	1.31	3.66	1.10	0.81	1.15	1.02	1.08	1.01
IL50×20×1.5N30	22.2	1.38	1.12	2.70	0.89	0.62	0.89	0.93	0.89	0.92
IL50×20×1.5N30-r	22.3	1.40	1.14	2.72	0.88	0.60	0.89	0.91	0.89	0.90
IL60×40×2.0N30	34.0	1.21	0.96	2.55	0.89	0.65	0.88	0.96	0.91	0.95
IL60×40×2.0N50	40.2	1.38	1.14	3.08	0.98	0.73	1.01	0.98	0.97	0.97
IL60×40×2.0N50-r	39.8	1.40	1.17	3.14	1.00	0.75	1.03	1.00	0.98	0.99
IL60×120×3.0N60	86.6	1.33	1.06	3.09	0.97	0.81	1.00	1.05	0.98	1.04
IL60×120×3.0N120	128.8	1.75	1.52	4.57	1.22	0.97	1.31	1.06	1.17	1.05
IL80×150×3.0N60	65.2	1.10	0.88	2.76	1.03	1.34	1.08	1.13	1.02	1.13
IL80×150×3.0N150	89.3	1.25	1.14	3.73	1.09	1.06	1.19	0.92	1.01	0.92
IL80×150×3.0N150-r	88.7	1.27	1.15	3.75	1.13	1.34	1.25	0.99	1.05	0.98
IL100×100×3.0N30	74.3	1.24	0.96	2.80	1.06	0.91	1.04	1.22	1.11	1.21
IL100×100×3.0N90	102.0	1.53	1.30	3.88	1.22	1.14	1.29	1.26	1.17	1.25
IL120×60×3.0N30	73.4	1.21	0.94	2.57	0.92	0.74	0.89	1.06	0.96	1.04
IL120×60×3.0N60	81.5	1.28	1.05	2.90	0.92	0.73	0.93	1.00	0.91	0.99
IL150×80×3.0N30	55.7	1.05	0.83	2.38	1.03	1.40	1.02	1.19	1.05	1.18
IL150×80×3.0N90	70.3	1.16	1.01	2.98	1.04	1.33	1.11	1.15	0.98	1.13
IL60×60×1.5N30	19.5	1.29	1.07	2.69	1.02	0.81	1.03	1.08	1.01	1.06
IL60×60×1.5N60	25.3	1.50	1.35	3.49	1.14	0.91	1.21	1.08	1.07	1.06
IL60×60×2.0N30	31.4	1.19	0.94	2.58	0.96	0.78	0.97	1.06	0.98	1.05
IL60×60×2.0N60	41.3	1.43	1.22	3.39	1.10	0.89	1.16	1.08	1.07	1.06
IL60×60×3.0N30	60.4	1.04	0.79	2.37	0.87	0.71	0.86	1.04	0.92	1.04
IL60×60×3.0N60	78.8	1.27	1.01	3.09	1.01	0.82	1.04	1.06	1.02	1.06
IL60×60×4.0N30	96.7	0.94	0.70	2.24	0.81	0.67	0.79	1.07	0.88	1.07
IL60×60×4.0N60	124.7	1.16	0.89	2.89	0.94	0.77	0.95	1.09	0.97	1.09
IL120×120×2.0N60	34.9	1.30	1.17	2.94	1.03	0.99	1.07	1.12	0.96	1.10
IL120×120×2.0N120	44.0	1.39	1.42	3.70	1.10	1.06	1.20	1.08	0.98	1.07
IL120×120×2.5N60	50.8	1.23	1.05	2.85	0.99	0.97	1.03	1.10	0.96	1.09
IL120×120×2.5N120	65.7	1.39	1.32	3.69	1.10	1.07	1.19	1.10	1.00	1.08
IL120×120×3.5N60	89.0	1.13	0.91	2.70	0.93	0.93	0.95	1.07	0.93	1.06
IL120×120×3.5N120	116.7	1.33	1.16	3.54	1.06	1.05	1.14	1.08	1.01	1.07

IL120×120×5.0N60	163.5	1.03	0.79	2.57	0.89	0.89	0.89	1.05	0.92	1.05
IL120×120×5.0N120	208.0	1.22	0.99	3.27	0.99	0.99	1.04	1.05	0.98	1.04
IL300×300×2.0N150	38.4	1.30	1.80	3.23	0.95	0.87	1.01	0.98	0.79	0.95
IL300×300×2.0N300	43.8	1.11	1.89	3.69	0.88	0.80	0.99	0.84	0.70	0.82
IL300×300×3.5N150	121.3	1.42	1.44	3.68	1.09	1.04	1.15	1.17	0.98	1.14
IL300×300×3.5N300	150.3	1.43	1.69	4.56	1.13	1.07	1.25	1.10	0.96	1.08
IL300×300×4.0N150	153.2	1.40	1.34	3.63	1.08	1.04	1.13	1.17	0.99	1.15
IL300×300×4.0N300	192.9	1.45	1.62	4.58	1.14	1.09	1.26	1.12	0.99	1.10
IL300×300×6.0N150	343.7	1.40	1.21	3.75	1.08	0.86	1.10	1.12	1.04	1.10
IL300×300×6.0N300	445.4	1.58	1.52	4.86	1.20	0.94	1.28	1.11	1.10	1.09
IL100×80×1.5N40	21.6	1.43	1.29	2.98	1.09	0.85	1.10	1.11	1.03	1.09
IL100×80×1.5N80	26.3	1.50	1.52	3.62	1.13	0.88	1.20	1.07	1.02	1.05
IL100×80×2.0N40	35.5	1.34	1.13	2.91	1.05	0.83	1.06	1.11	1.03	1.09
IL100×80×2.0N80	44.5	1.50	1.38	3.65	1.14	0.90	1.20	1.10	1.06	1.08
IL100×80×2.5N40	51.3	1.26	1.02	2.81	1.00	0.81	1.01	1.09	1.01	1.07
IL100×80×2.5N80	65.3	1.45	1.27	3.58	1.11	0.89	1.16	1.10	1.06	1.09
IL100×80×3.0N40	69.9	1.20	0.94	2.75	0.97	0.79	0.97	1.08	1.00	1.07
IL100×80×3.0N80	88.8	1.40	1.18	3.48	1.09	0.87	1.13	1.09	1.06	1.08
IL200×150×2.0N75	36.5	1.38	1.42	3.08	1.05	0.99	1.09	1.13	0.95	1.10
IL200×150×2.0N150	40.7	1.28	1.51	3.42	0.98	0.92	1.07	1.00	0.84	0.97
IL200×150×2.5N75	55.1	1.35	1.27	3.09	1.05	1.01	1.08	1.15	0.97	1.13
IL200×150×2.5N150	66.7	1.39	1.49	3.75	1.08	1.03	1.16	1.11	0.95	1.09
IL200×150×4.0N75	121.4	1.19	1.00	2.88	0.97	0.95	0.99	1.10	0.95	1.09
IL200×150×4.0N150	154.4	1.36	1.24	3.66	1.07	1.04	1.14	1.13	1.00	1.11
IL200×150×4.5N75	168.3	1.27	1.04	3.13	1.01	0.81	1.01	1.09	1.01	1.07
IL200×150×4.5N150	213.1	1.46	1.29	3.97	1.11	0.88	1.16	1.10	1.06	1.09
IL400×200×3.0N100	81.8	1.48	1.65	3.29	1.09	1.01	1.11	1.14	0.98	1.11
IL400×200×3.0N200	97.9	1.50	1.90	3.94	1.10	1.02	1.17	1.14	0.94	1.12
IL400×200×4.0N100	135.7	1.38	1.34	3.22	1.06	1.01	1.07	1.14	0.99	1.12
IL400×200×4.0N200	167.1	1.48	1.60	3.97	1.12	1.05	1.18	1.19	0.99	1.16
IL400×200×6.0N100	300.8	1.32	1.14	3.28	1.04	0.81	1.02	1.08	1.02	1.06
IL400×200×6.0N200	377.8	1.50	1.40	4.12	1.13	0.88	1.17	1.14	1.06	1.12
IL400×200×8.0N100	482.4	1.19	0.97	3.07	0.97	0.77	0.95	1.05	0.99	1.03
IL400×200×8.0N200	611.8	1.40	1.21	3.89	1.08	0.86	1.11	1.12	1.05	1.10
Mean		1.36	1.23	3.34	1.04	0.92	1.09	1.09	1.00	1.07
COV		0.150	0.227	0.182	0.099	0.179	0.118	0.073	0.097	0.073
Resistance factor, ϕ		0.70	0.70	0.91	0.90	0.80	0.80	0.85	0.85	0.85
Reliability index, β		4.15	3.25	5.87	2.56	2.17	3.07	3.04	2.63	2.98

Note: # means using IOF design equation; * means using ITF design equation.

Table 10: Coefficients for web crippling design of cold-formed steel sections using modified unified design equation

Provision	Steel	Section type	Load condition	Coefficients					Limits ($\theta = 90^{\circ}$)			
				C	C_R	C_N	C_h	ϕ	r_i/t	N/t	h/t	N/h
NAS [24]	Carbon steel	Single web channel	IOF	13.0	0.23	0.14	0.01	0.90	≤ 5.0	≤ 210	≤ 200	≤ 2.0
			ITF	24.0	0.52	0.15	0.001	0.80	≤ 3.0	≤ 210	≤ 200	≤ 2.0
Zhou and Young [25]	Duplex stainless steel	Square and rectangular hollow sections	IOF	7.0	0.21	0.26	0.001	0.70	≤ 2.0	≤ 50	≤ 50	≤ 2.0
			ITF	7.0	0.11	0.24	0.001	0.70	≤ 2.0	≤ 50	≤ 50	≤ 2.0
			IL	15.3	0.26	0.08	0.003	0.80	≤ 2.0	≤ 50	≤ 200	≤ 1.6
Proposed	Lean duplex stainless steel		IOF	8.0	0.21	0.26	0.001	0.85	≤ 2.0	≤ 150	≤ 145	≤ 1.5
			ITF	8.3	0.21	0.26	0.001	0.85	≤ 2.0	≤ 150	≤ 145	≤ 1.5
			IL	9.1	0.21	0.26	0.001	0.85	≤ 2.0	≤ 150	≤ 145	≤ 1.5

Note: The table is suitable to stiffened or partially stiffened flanges that unfastened to support.

Table 11: Coefficients for web crippling design of cold-formed stainless steel sections using modified direct strength method

Provision	Load condition	a	b	n	λ_k	γ	ϕ
Li and Young [31,32]	IOF	0.93	0.30	0.41	0.600	0.77	0.85
	ITF	0.73	0.01	0.35	0.480	1.20	0.85
	IL	0.88	0.09	0.35	0.515	1.20	0.85
Proposed	IOF	0.87	0.11	0.35	0.600	1.05	0.85
	ITF	0.89	0.17	0.35	0.600	1.05	0.85
	IL	0.91	0.11	0.35	0.600	1.10	0.85

Note: The table is suitable to stiffened or partially stiffened flanges that unfastened to support.
The proposed coefficients apply when $10 \leq h/t \leq 145$, $r_i/t \leq 2.0$, $N/t \leq 150$, $N/h \leq 1.5$ and $\theta = 90^{\circ}$.